Geosci. Model Dev. Discuss., 7, 4931–4992, 2014
www.geosci-model-dev-discuss.net/7/4931/2014/
doi:10.5194/gmdd-7-4931-2014

Geoscientific Model Development Discussions
Open Access

A simplified permafrost-carbon model for long-term climate studies with the CLIMBER-2 coupled earth system model

K. A. Crichton[1,2], D. M. Roche[3,4], G. Krinner[1,2], and J. Chappellaz[1,2]

[1]CNRS, LGGE (UMR5183), 38041 Grenoble, France
[2]Univ. Grenoble Alpes, LGGE (UMR5183), 38041 Grenoble, France
[3]CEA/INSU-CNRS/UVSQ, LSCE (UMR8212), Centre d'Etudes de Saclay CEA-Orme des Merisiers, bat. 701 91191 Gif-sur-Yvette Cedex, France
[4]Cluster Earth and Climate, Department of Earth Sciences Faculty of Earth and Life Sciences, Vrije Universiteit Amsterdam De Boelelaan 1085, 1081 HV Amsterdam, the Netherlands

Received: 27 June 2014 – Accepted: 16 July 2014 – Published: 30 July 2014

Correspondence to: K. A. Crichton (kcrichton@lgge.obs.ujf-grenoble.fr)

Published by Copernicus Publications on behalf of the European Geosciences Union.

Abstract

We present the development and validation of a simplified permafrost-carbon mechanism for use with the land surface scheme operating in the CLIMBER-2 earth system model. The simplified model estimates the permafrost fraction of each grid cell according to the balance between modelled cold (below 0 °C) and warm (above 0 °C) days in a year. Areas diagnosed as permafrost are assigned a reduction in soil decay, thus creating a slow accumulating soil carbon pool. In warming climates, permafrost extent reduces and soil decay increases, resulting in soil carbon release to the atmosphere. Four accumulation/decay rate settings are retained for experiments within the CLIMBER-2(P) model, which are tuned to agree with estimates of total land carbon stocks today and at the last glacial maximum. The distribution of this permafrost-carbon pool is in broad agreement with measurement data for soil carbon concentration per climate condition. The level of complexity of the permafrost-carbon model is comparable to other components in the CLIMBER-2 earth system model.

1 Introduction

Model projections of climate response to atmospheric CO_2 increases predict that high northern latitudes experience amplified increases in mean annual temperatures compared to mid-latitudes and the tropics (Collins et al., 2013). The large carbon pool locked in permafrost soils of the high northern latitudes (Tarnocai et al., 2009) and its potential release on thaw (Schuur et al., 2008; Harden et al., 2012) make permafrost and permafrost related carbon an important area of study. Thus far permafrost models that have been coupled within land-surface schemes have relied on thermal heat diffusion calculations from air temperatures into the ground to diagnose permafrost location and depth within soils (Koven et al., 2009; Wania et al., 2009a; Dankers et al., 2011; Ekici et al., 2014). This approach requires a good physical representation of topography, soil types, snow cover, hydrology, soil depths and geology to give a reliable output

GMDD
7, 4931–4992, 2014

(Riseborough et al., 2008). The physically based approach lends itself to smaller grid cells and short timescale snapshot simulations for accuracy of model output. The aim of this work is to develop a simplified permafrost-carbon mechanism that is suitable for use within the CLIMBER-2 earth system model (Petoukhov et al., 2000; Ganopolski et al., 2001), and also suitable for long timescale experiments. The CLIMBER-2 model with a coupled permafrost-carbon mechanism, combined with proxy marine, continental and ice core data provide a means to model the past dynamic contribution of permafrost-carbon within the carbon cycle.

1.1 Physical permafrost modelling

Several land surface models diagnose permafrost and concomitant higher soil carbon concentrations (Wania et al., 2009a, b; Koven et al., 2009; Dankers et al., 2011). These models are usually driven with climatic variables output from global climate models (GCMs) and grid cell sizes are the order of 2.5° (the order of hundreds of km) for global simulations. These models use surface air temperature and thermal diffusion calculations to estimate the soil temperature at depths, and from this the depth at which water freezes in the soil. An active layer thickness (ALT) can be determined from this, and soil carbon dynamics are calculated for the unfrozen parts of the soil. These land surface models may also include a representation of peatlands (Sphagnum dominated areas, and wetlands), which store an estimated 574 Gt C in northern peatlands (Yu et al., 2010), of which a large part are located within the permafrost region (Northern Circumpolar Atlas: Jones et al., 2009). The dynamic response of carbon in permafrost soils subject to (rapid) thaw is not well constrained (Schuur et al., 2011) and field studies and modelling studies still seek to better constrain this. Riseborough et al. (2008) reviewed advances in permafrost modelling identifying that modelling of taliks (pockets or layers of thawed soil at depth which do not refreeze in winter) complicates physical modelling. The importance of soil depth (lower boundary conditions) was also highlighted, Alexeev et al. (2007) demonstrated that the longer the simulation, the larger the soil column depth required in order to produce reliable thermal diffusion-based

GMDD
7, 4931–4992, 2014

temperature calculations: a 4 m soil depth can produce reliable temperature predictions for a 2 year simulation, and for a 200 year simulation a 30 m soil depth would be required. Van Huissteden and Dolman (2012) reviewed Arctic soil carbon stocks estimates and the permafrost-carbon feedback. They note the processes by which carbon loss occurs from thawing permafrost including active layer thickening (also caused by vegetation disturbance), thermokarst formation, dissolved organic carbon (DOC) export, fire and other disturbances. Their conclusions were that "current models are insufficiently equipped to quantify the carbon release at rapid thaw of ice-rich permafrost" which within a model would require accurate representation of local topography, and hydrology as well as a-priori knowledge of the ice-content in the soils. Koven et al. (2013) further highlighted the importance of soil depths and of soil and snow dynamics on the accuracy of permafrost extent in CMIP (coupled model intercomparison project) models. The high computing power requirements of physical models at grid sizes where output could be an acceptable confidence level makes these kind of models currently unsuitable for long timescale dynamically coupled modelling studies. Current CMIP model projections of future climate reported by the IPCC (Stocker et al., 2013) do not include a possible feedback mechanism from permafrost-soils.

1.2 Past permafrost carbon

Zimov et al. (2009) created a physical model for carbon dynamics in permafrost soils. This 1 dimensional model was intended to simulate the carbon dynamics specifically in the permafrost region. Carbon input to the soil originates from root mortality and aboveground litter transport via organic carbon leaching and mixing by bioturbation and cryoturbation. Loss of carbon from the soils occurs via decomposition. The frozen soil active layer depth also determines the maximum root depth of vegetation. Modelled soil carbon profiles were similar to those found in present day ground data for similar conditions. Results of experiments where the temperature zone was changed linearly from Temperate to Cold, then snapped back to Temperate (mimicking a glaciation then termination in Europe) demonstrated the characteristic of slow carbon accumulation

GMDD
7, 4931–4992, 2014

in permafrost soils, and fast carbon release on thaw. An important result of this study was that the main driver of the high carbon content in the frozen soils was the low decomposition rates, which reduce further with depth in the soil column, as a result of permafrost underlying an active layer which cycles between freezing and thawing in the year. To estimate the amounts of carbon stored on the land and the ocean at LGM, Ciais et al. (2012) used δ^{18}O data and carbon cycle modelling to calculate gross primary productivity (GPP) at LGM and in the present day. They estimate that the total land carbon stocks had increased by 330 Gt C since LGM, but that 700 Gt C less was presently stored as inert land carbon stocks compared to LGM. Zech et al. (2011) studying two permafrost-loess paleosol sequences concluded that on glacial timescales the effect of reduced biomass productivity may be of secondary importance to the effect of permafrost preserving soil organic matter when considering total land carbon stocks. The Ciais et al. (2012) inert land carbon stock may represent this permafrost carbon pool.

1.3 Carbon cycle responses during a deglaciation

The current leading hypothesis for the fast rise in atmospheric CO_2 in the last glacial termination (17.5 to 12 kyr BP) (Monnin et al., 2001) is that carbon was outgassed from the ocean via a reorganisation of ocean circulation that released a deep carbon store in the Southern ocean (Sigman et al., 2010; Fischer et al., 2010; Shakun et al., 2012). The Zimov et al. (2009) model, Ciais et al. (2012) and the δ^{13}C record for the last termination (Lourantou et al., 2010; Schmitt et al., 2012) suggest that permafrost may have had a role to play in the dynamics of the carbon cycle during the last termination. At the start of termination 1, the end of the last glacial maximum and the transition to the present interglacial climate, a fast drop in the δ^{13}C of the atmosphere was seen from ice core data. Soil carbon has a δ^{13}C signature depleted by around 18 ‰ compared to the atmosphere (Maslin and Thomas, 2003), a release of carbon from thawing permafrost soils is a possible explanation for the δ^{13}C record.

In this study, we aim to develop a permafrost-carbon model for long-term paleoclimate studies. We present the development of the permafrost-carbon model and

GMDD
7, 4931–4992, 2014

validate it with present-day ground measurement data for soil carbon concentrations in high northern latitude soils.

2 Model development

2.1 CLIMBER-2 standard model

The CLIMBER-2 model (Petoukhov et al., 2000; Ganopolski et al., 2001) consists of a statistical-dynamical atmosphere, a 3-basin averaged dynamical ocean model with 21 vertical uneven layers and a dynamic global vegetation model, VECODE (Brovkin et al., 1997). The model version we use is as Bouttes et al. (2012) and Brovkin et al. (2007). The model can simulate around 20 kyr in 10 h (on a 2.5 GHz processor) and so is particularly suited to palaeoclimate and long timescale fully coupled modelling studies. The version of CLIMBER-2 we use (Bouttes et al., 2009, 2011, 2012) is equipped with a carbon-13 tracer in its global carbon cycle model, ice sheets and carbonate compensation in ocean waters (Brovkin et al., 2007) as well as ocean biochemistry. The ice sheets are determined by scaling ice sheets size between the Last Glacial Maximum (LGM) condition from Peltier (2004) and the Pre-Industrial (PI) ice sheet using the sea level record to determine land ice volume (Bouttes et al., 2012). The dynamic vegetation model has two plant functional types (PFTs); trees and grass, plus bare ground as a dummy type. It has two soil pools; "fast" and "slow" representing litter and humus respectively. Soils have no depth, and are only represented as carbon pools. The carbon pools of the terrestrial vegetation model are recalculated once every year. The grid cell size of the atmospheric and land surface models are approximately 51° longitude (360/7°) by 10° latitude. Given the long time-scale applications of the CLIMBER-2 model and the very large grid size for both atmosphere and land, none of the existing approaches of modelling permafrost are suitable. Thermal diffusion based physical models would produce results with unacceptable uncertainties (error bounds) compounding over long timescales. To create the permafrost model for CLIMBER-2,

GMDD
7, 4931–4992, 2014

the driving mechanism creating high soil carbon concentrations is a reduced soil decay rate in the presence of permafrost, identified by Zimov et al. (2009) as a primary driver in soil carbon accumulation.

2.2 Permafrost-carbon mechanism

CLIMBER-2 grid cells for the land surface model are very large. Two options are available to diagnose permafrost location: either by creating a sub-grid within the land grid or by diagnosing a fraction of each grid cell as permafrost which is the approach followed here. Figure 1 shows a schematic representation of a CLIMBER-2 grid cell, and how the permafrost fraction of the land is defined relative to other cell parameters when permafrost is diagnosed as a fraction of each cell. For the carbon cycle the calculations of carbon fluxes between atmosphere and land grid cells are for the cell mean. Each grid cell contains cell-wide soil-carbon pools (fast soil or slow soil, per plant functional type), so to account for permafrost-soils either a new permafrost-soil pool needs to be created for each grid cell, or permafrost soils can be mixed back into the standard soil pools at every time-step (Fig. 2a). If the land grid is downscaled a third option is available, were each sub-grid cell maintains an individual soil carbon pool (Fig. 2b). This, however, requires an increase in computational time which slows down the run speed of the model.

The soil carbon in CLIMBER-2 is built from vegetation mortality and soil carbon decay is dependent on surface air temperature, the total amount of carbon in the pool and the source of carbon (i.e. trees or grass). This is shown in Eqs. (1) and (2), where δt is the model time step taken as 1 year for the land vegetation carbon-cycle.

$$\text{Soil carbon respired} = \frac{C_{\text{pool}}}{\tau} \cdot \delta t \tag{1}$$

$$\tau = c \cdot e^{-(\text{ps5}(T_{\text{mat}} - T_{\text{soil}}))} \tag{2}$$

The characteristic soil decay time, τ, is dependent upon the mean annual surface air temperature (T_{mat}), the temperature of the soil (T_{soil}) and two constants c and ps5.

GMDD
7, 4931–4992, 2014

The term ps5 is fixed at 0.04. The value of c is dependent upon the soil carbon type, being 900 for all slow soils, 16 for fast tree PFT (plant functional type) soil and 40 for fast grass PFT soil. The destruction times (decay rates) for organic residue (soils) are most strongly based on soil microbial activity and the relative amount of lignin in the residues (Aleksandrova, 1970; Brovkin et al., 1997). Increasing the residence time of carbon in permafrost affected soils reduces the decay rates and results in higher soil carbon concentrations. We chose to modify the residence time, τ, in the presence of permafrost using:

$$\tau_{\text{perma}} = \tau(a \cdot F_{\text{sc}} + b) \tag{3}$$

Where a and b are tuneable dimensionless constants, F_{sc} is frost index, a value between 0 and 1, which is a measure of the balance between cold and warm days in a year, and is shown in Eq. (4) where DDF are degree-days below 0 °C and DDT are degree-days above 0 °C in a year for daily average surface air temperature (Nelson and Outcalt, 1987). Snow cover acts to insulate the ground against the coldest winter temperatures and reduces permafrost extent (Zhang, 2005; Gouttevin et al., 2012). The subscript sc in Eqs. (3) and (4) indicate that these values are corrected for snow cover and represent the ground–snow interface conditions not the snow surface–air interface conditions.

$$F_{\text{sc}} = \frac{\text{DDF}_{\text{sc}}^{(1/2)}}{\text{DDF}_{\text{sc}}^{(1/2)} + \text{DDT}^{(1/2)}} \tag{4}$$

Including the frost-index as a multiplier for the permafrost soils carbon residence time was needed to make the model more tunable and so more controllable for global soil carbon content. The decay rates of soil carbon in permafrost affected cells are dependent on mean annual temperature, as with non-permafrost cells. They are also dependent upon the fractional cover of permafrost in the cell and the frost index, a measure of the severity of coldness in a year.

GMDD
7, 4931–4992, 2014

2.3 1-D model

We first developed a one dimensional model to test the effect the different assumptions made for the model design. The total carbon stock in a grid cell using each method (sub-grid and re-mixing) was compared for equilibrium soil carbon concentration. The carbon input from vegetation mortality is the same for both the re-mixing and the sub-grid model, as is rainfall. The variables of permafrost fraction, mean annual air surface temperature (MAAT) and frost index are varied one at a time to compare the model outputs. The constants a and b for Eq. (3) were both set to 20 for fast soils and 2 for slow soils for the permafrost soils, and as the standard model for the non-permafrost soils. These values for a and b were chosen to compare the performance of the two methods, not for accurate soil carbon concentrations.

Figure 3 shows the results of sensitivity experiments comparing these two approaches for one CLIMBER-2 land grid cell. Baseline settings of permafrost fraction = 0.6, Frost index = 0.6, mean annual air temperature = −10 °C have a relative soil carbon concentration of 1. The sub-grid method outputs a linear-type relationship between permafrost fraction and soil carbon stored. The re-mixing model outputs lower soil carbon concentration for lower fractional permafrost coverage rising quickly when permafrost fraction approaches 1. For the air temperature as variable, the two approaches show a similar response. For higher frost index the soil carbon concentration increases, with the sub-grid method showing slightly more sensitivity than the re-mixing model.

2.4 1-D model vs. real world

In the real world case, the three variables used to drive the 1-D model are not independent of each other. An increasing permafrost fraction would normally be associated with an increasing frost-index (Nelson and Outcalt, 1987) and a decreasing mean annual air temperature. Figure 4 shows a schematic representation of a permafrost gradient (Fig. 4a) and for three grid cells, with 20, 50 and 100 % permafrost

GMDD
7, 4931–4992, 2014

coverage (Fig. 4b). As permafrost coverage reduces, ALT (active layer thickness) increases, with continuous-zone permafrost having mean ALT less than half that of discontinuous/sporadic-zone permafrost (Jones et al., 2009). This active layer is where soil accumulation and decay can occur in the warm season. In general, continuous permafrost is located further north and in more extreme climate conditions, resulting in a shorter warm season. The soil decay rate in discontinuous or isolated region permafrost will be higher than the soil decay rate in the continuous zone, even if carbon input to the soil is equal for both. This would result in a non-linear relationship between equilibrium soil carbon content for increasing permafrost cover, shown in Fig. 4c, which is for the constant MAAT, constant F_{sc} condition.

2.5 CLIMBER-2 modelled NPP

The comparisons of the sub-grid to re-mixing approaches shown in Fig. 3 take no account of reductions in input to soils via NPP in colder climates. Figure 5 shows the CLIMBER-2 modelled NPP and the MODIS 2000–2005 mean NPP product (Zhao et al., 2011) for the present-day (PI, pre-industrial for CLIMBER output). The CLIMBER-2 vegetation model shows NPP patterns similar to the MODIS dataset. The boreal forest belt seen at around 60° N in the MODIS set is not clearly seen in the CLIMBER-2 model, mainly due to the large grid cell size. In Siberia and Alaska the NPP in CLIMBER-2 is does not appear to be overestimated. The reduced NPP in the coldest regions would tend to reduce soil carbon accumulation via reduced input from plant mortality (this is shown schematically in Fig. 4c). In order to test the applicability of the CLIMBER-2 model for the glacial climate, a comparison of NPP for the LGM with a more complex model can be done. Figure 6 shows LGM(eq) NPP for LPX (data courtesy M. Martin-Calvo, Prentice et al., 2011) and for CLIMBER-2 for an LGM climate. At LGM the NPP in Siberia and the coldest permafrost regions are non-zero in both models, and CLIMBER-2 follows the same general patterns as LPX predicts. CLIMBER-2 shows slightly lower NPP in the southern parts of Russia, possibly similar to the boreal forest belt that is not well represented in the pre-indusrial climate background NPP due

GMDD
7, 4931–4992, 2014

to the large grid cell size. Overall at both periods, PI and LGM, CLIMBER-2 represents NPP reasonably well.

Considering the added effects of soil carbon input, warm season length and active layer thickness for the 1-D model, the re-mixing model better represents a real-world case although the increase in carbon concentration between 90–100 % permafrost is probably exaggerated. The sub-grid model would underestimate the carbon accumulation in higher permafrost-coverage grid cells. A sub-grid method for permafrost-carbon would also require more extensive model modifications and would slow down computational speed. The more simple model, the re-mixing model, where the entire grid cell sees increased carbon concentration, requires fewer assumptions on processes controlling carbon accumulation and decay. For these reasons we selected the re-mixing model to implement into CLIMBER-2.

3 CLIMBER-2 permafrost-carbon model

We implemented Eq. (3) into CLIMBER-2 using the re-mixing model. In order to study the effect of different carbon accumulation and release rates (the permafrost-carbon dynamics) in later modelling studies the decay rates can be tuned to distribute the carbon more into the fast pool (making a quickly responding soil carbon pool) or more into the slow pool (making a more slowly responding soil carbon pool). A total of 4 dynamic settings are retained for later coupled climate studies.

3.1 Simulated climates to tune the permafrost-carbon model

Three simulated climates were used to tune and validate the permafrost-carbon model: an LGM equilibrium climate: LGM(eq), a PI equilibrium climate: PI(eq), and a PI transient climate: PI(tr) obtained at the end of a transient deglaciation from the LGM climate. These three climates allow the total soil carbon to be tuned to the estimates

GMDD
7, 4931–4992, 2014

of Ciais et al. (2012) for the LGM and PI climate conditions, these are described in Table 1.

Frost-index cut off to match present-day areal permafrost extent

In order to obtain a relationship between calculated frost-index and the permafrost-fraction of a grid cell, measurement and ground data for frost index and permafrost location were used. For present-day mean daily surface air temperatures, the freeze and thaw indices values on a 0.5° global grid were obtained from the National Snow and Ice Data Centre (NSIDC) database (Zhang, 1998). Using these values for freeze and thaw index a global frost index dataset on a 0.5° grid scale was created using Eq. (4). The present-day estimates of land area that are underlain by permafrost are provided by Zhang et al. (2000), using the definition of zones: "continuous" as 90–100 % underlain by permafrost, "discontinuous" as 50–90 % underlain by permafrost, "sporadic" as 10–50 % permafrost and "isolated" as less than 10 %. Zhang et al. (2000) used these zonations to provide area estimates of the total land area underlain by permafrost. Summing the total land area that has a frost index higher than a particular value and comparing this to the Zhang et al. (2000) estimate can identify the appropriate boundary between permafrost and non-permafrost soils. Figure 7 shows the Zhang et al. (2000) permafrost areas for the high, medium and low ranges defined by the high, medium and low % estimates of permafrost zones marked as horizontal lines. The land area indicated by green squares is the total land surface in the Northern Hemisphere which has a frost-index value higher (where higher indicates a colder climate) than the cut-off value shown on the *x* axis. Here the frost-index cut-off value of 0.57 shows good agreement with the medium (mean) estimate of the Zhang et al. (2000) total area of land underlain by permafrost.

GMDD
7, 4931–4992, 2014

3.2 Geographic permafrost distribution for the present-day

Figure 8 shows, coloured in blue, the land grid cells with a frost-index higher than 0.57 for 0.5° grid, with the north located at the centre of the map. Overlaid on this map area are the limits of the permafrost zones defined by the International Permafrost Association (IPA) (Jones et al., 2009). The frost-index value cut-off at 0.57 results in a southern limit of permafrost that represents approximately the middle of the discontinuous zone with some areas showing better agreement than others.

Figure 9 represents the upscaling of the 0.5° datasets for frost index and permafrost coverage to the CLIMBER-2 land grid scale. It shows the percentage of land in each CLIMBER-2 size grid cell defined as permafrost, according to the 0.57 frost-index cut-off value shown in Fig. 8, plotted against the mean value of frost-index for the same grid cell. Circled points in Fig. 9 are where the grid cell has a large fraction of ocean (more than 75 %), and the milder ocean temperatures in winter reduce the mean frost-index value of the whole grid cell. The dashed line shows a well-defined sigmoid-type function that relates frost index to permafrost percentage of the land. We employ this relationship to predict permafrost area in CLIMBER-2, as the frost-index can be calculated within the model from modelled daily temperatures. Permafrost fraction is thus modelled as:

$$P_{\text{landfraction}} = A\frac{0.976+\beta}{\sqrt{1+\beta^2}} - 0.015 \quad (5)$$

Where A and β are defined in Table 2 and the model described in Sect. 3.4. Frost index is calculated from modelled daily surface temperatures and corrected for snow-cover. The snow correction in our model is done using a simple linear correction of surface-air temperature, using snow thickness to estimate the snow–ground interface temperature. This correction is based on data from Taras et al. (2002). The snow correction performs reasonably well in CLIMBER-2 compared to measurement data from Morse and Burn (2010) and Zhang (2005). This is because the large grid-cell size results in non-extreme snow depths and air surface temperatures. The snow correction

GMDD
7, 4931–4992, 2014

is described in Appendix A. Equation (6) shows this linear model for snow correction, which is only applied for surface air temperatures lower than −6 °C. This snow–ground interface temperature is used to calculate the freeze index (DDF_{sc}) in Eq. (4).

$$T_{g.i.} = T_{surf} - \frac{(T_{surf} + 6) \cdot SD}{100} \quad (6)$$

Where $T_{g.i.}$ is ground interface temperature (°C), T_{surf} is surface air temperature (°C) and SD is snow depth (cm). Overall the effect of the snow correction within the model produced a maximum decrease in permafrost area of 8 % (compared to the uncorrected version) in the most affected grid cell for the PI(eq) simulation and is therefore significant.

3.3 Permafrost extent tuning

Using the snow-corrected frost-index value, four permafrost extent models representing the range of values for permafrost area from Zhang et al. (2000) were determined. The model settings are shown in Table 2 and refer to A and β from Eq. (5). $P_{landfraction}$ is limited between 0 and 1, and the functions are plotted in Fig. 10. These settings were identified by adjusting the sigmoid function to obtain total permafrost area values at the PI(eq) simulation similar to the Zhang et al. (2000) areal estimates of permafrost and to maximise the difference in area between the PI(eq) and LGM(eq) simulations permafrost extent. More complex models underestimate permafrost extent at LGM (Levavasseur et al., 2011; Saito et al., 2013) quite significantly and so by maximising the difference between PI and LGM permafrost, we reduce the underestimate as far as possible of LGM permafrost extent.

3.4 Tuning the soil-carbon model

Soil carbon concentration is controlled by the balance between soil carbon uptake and soil carbon decay. There are four soil-carbon pools in CLIMBER-2; fast soil: trees derived (ft) and grass derived (fg), slow soil: trees derived (st) and grass derived (sg).

GMDD
7, 4931–4992, 2014

The final soil-carbon pool dynamics per grid cell are calculated based on the fractional cover of trees and grass in the grid cell and soil accumulation and decay. In transient climate conditions the changes in soil carbon concentration is dependent upon the relative trend of the uptake and decay rates. The slow carbon pools have a slower decay rate than the fast carbon pools, so if there is more carbon in the fast pool than in the slow pool this carbon can be lost more quickly to the atmosphere via decay. This will apply more strongly in permafrost-thaw conditions. When permafrost thaws, that high carbon soil will see increased decay rates and fast soils will loose carbon more quickly than slow soils. The tunable constants a and b (Eq. 3) can be independently tuned for fast and slow soils, so carbon can be placed relatively more in the fast (slow) pools as desired. This results in permafrost carbon that decays more quickly (more slowly) when the permafrost thaws. It also results in carbon accumulation rates in the permafrost soils being faster (slower).

At LGM, the area of permafrost on land was larger than today (Vandenberghe et al., 2012) but not much information on soil carbon has been conserved, especially if it has long since decayed as a result of permafrost degradation during the last termination. To constrain the total carbon content in permafrost soils we use the estimates of Ciais et al. (2012), for total land carbon these are 3640 ± 400 Gt C at LGM and 3970 ± 325 Gt C at PI, with a total change of +330 Gt C between LGM and PI. The standard CLIMBER-2 model predicts total land carbon stocks of 1480 Gt C at LGM and 2480 Gt C at PI, showing good agreement with the active-land-carbon estimates of Ciais et al. (2012) (of 1340 ± 500 Gt C LGM and 2370 ± 125 Gt C PI). Any "new" soil carbon is created via the permafrost-carbon mechanism and is assumed to be equivalent to the inert land carbon pool estimates of Ciais et al. (2012). However, the dynamic behaviour of permafrost-carbon in changing climates is not well constrained and it is for this reason that a set of four dynamic settings were sought. Here the "speed" of the dynamic setting is determined by the ratio of total fast pool to slow pool carbon (fp / sp), with "slow" being fp / sp < 0.5, "medium" being fp / sp 0.5 to 1, "fast" being fp / sp 1 to 1.5 and "extra-fast" being fp / sp > 1.5 for the PI-equilibrium simulation. The variables

GMDD
7, 4931–4992, 2014

"*a*" and "*b*" shown in Eq. (3) were set and each setting used for a PI(equilibrium), LGM(equilibrium) and PI(transient) simulation to identify the settings which resulted in total land carbon pools in agreement with the Ciais et al. (2012) estimates.

The LGM is conventionally defined as being the period around 21 kyr BP, when large parts of north America were underneath the Laurentide ice sheet. According to their time-to-equilibrium (the slow carbon accumulation rate) soils in this location, now free of ice, may not yet have reached equilibrium by the present day. Further than this, climate has changed significantly since the LGM so permafrost soils anywhere may not be currently in equilibrium (Rodionow et al., 2006), again due to its slow carbon accumulation rates. Due to this the PI(tr) simulation model output for total land carbon was used to tune the total land carbon stocks, as it includes a receding Laurentide ice sheet. At LGM, ice sheets were at maximum extent, so the problem of land being newly exposed does not occur in the model. For this reason, the LGM(eq) simulation is used to tune total land carbon for the LGM.

Details of the tuning for total land carbon stocks are available in Appendix B. It was found that only one area setting: the LOW–MEDIUM area provided an acceptable range of dynamic settings, as defined by the ratio of fast to slow soil carbon. The four selected dynamics settings are shown in more detail in Fig. 11, for total land carbon stock, atmospheric CO_2 and ratio of fast to slow soil-carbon pool. The *a* and *b* values for these settings are shown in Table 3.

To evaluate the effect of the different dynamic settings we ran an equilibrium PI simulation for all four selected settings for 40 kyr, followed by a permafrost switch-off for a further 10 kyr. Figure 12 shows the global total land carbon stocks for this experiment. The period between 0–40k simulation years demonstrate the transient effects of the slow accumulation rates in permafrost soils. Depending on the dynamic setting, the total land carbon takes more than 40 kyr to fully equilibrate in PI climate conditions. On permafrost switch-off, from 40k sim years, the soil-carbon previously held in permafrost soils is quickly released to the atmosphere, at a rate dependent upon the dynamic setting. The xfast setting releasing all excess carbon within hundreds of years and the

GMDD
7, 4931–4992, 2014

slow setting around 8000 years after total permafrost disappearance. Currently, the most appropriate carbon dynamic setting is unconstrained by measurement data. It is for this reason that these four settings cover such a large range of dynamic responses of soil carbon on permafrost thaw, to study the carbon dynamics in future experiments.

4 Model validtion

Hereafter, the name "CLIMBER-2P" denotes the model in which the permafrost-carbon mechanism operates fully coupled within the dynamic vegetation model.

4.1 Permafrost areal coverage and spatial distribution

Figure 13a shows the spatial pattern of permafrost as predicted in CLIMBER-2P with the snow correction included for the LOW–MEDIUM area setting. The modelled PI(tr) permafrost extent fairly well estimates the location of the present-day southern boundary of the discontinuous permafrost zone (Jones et al., 2009), with overestimate of permafrost extent in the western Siberian grid cell, and underestimate over the Himalayan plateau. Total permafrost area extent is shown in Table 4.

Comparing this to performance of other models (Levavasseur et al., 2011), the PI(eq) total permafrost area is closer to Zhang et al. (2000) estimates, but it must be kept in mind that for CLIMBER-2P the area was tuned to be in agreement with mean estimate from Zhang et al. (2000). The PI(tr) total permafrost area is higher by around 4×10^6 km^2 compared to the PI(eq). This is due to the North Pacific region being colder in PI(tr) than that of the PI(eq) simulation, and may be related to the land run-off, which is kept at LGM settings for the transient simulations. For LGM period, the best PMIP2 model in the Levavasseur study (interpolated case) underestimated total permafrost area by 22 % with respect to data estimates (of 33.8×10^6 km^2), and "worst" model by 53 %, with an all-model-median value of 47 % underestimate. The LOW–MEDIUM

GMDD
7, 4931–4992, 2014

CLIMBER-2P setting gives an LGM total permafrost area underestimate of around 40 %, slightly better than the median for PMIP2 models' permafrost area.

Figure 13b shows the LGM CLIMBER-2P permafrost extent with the reconstructed continuous and discontinuous southern boundaries (Vandenberghe et al., 2012; French and Millar, 2013) overlaid. In the LGM simulation for CLIMBER-2P, coastlines do not change so the Siberian Shelf and other exposed coastlines in the northern polar region are not included in the CLIMBER-2P permafrost area estimate. These coastal shelves cover an estimated area of 5 to 7×10^6 km^2. Another area which is not diagnosed as permafrost in CLIMBER-2P is the Tibetan plateau, which would be an additional estimated 6×10^6 km^2. If these two regions were added (totalling around 12×10^6 km^2) to the LGM area estimate it would bring the modelled permafrost area (then totalling around 33×10^6 km^2) much closer to the data estimate as reported in the Levavasseur et al. (2011) study. The permafrost extent model is dependent upon the CLIMBER-2P modelled climate. The very large grid cell size of CLIMBER-2P means that modelled mountainous regions such as the Tibetan plateau are problematic, resulting in a possible too-warm climate (compared to the real-world) in this region.

4.2 Soil carbon dynamics

Accumulation rates show general agreement with the Zimov et al. (2009) model and the Wania et al. (2009b) (LPJ) model. Figure 14 shows output for the "medium" permafrost dynamic for the PI (equilibrium) spin-up. The Northern European Russia site can be compared to the the Ayaha-Yacha location from the Wania et al. (2009b) and to the extra-cold and wet–dry conditions from Zimov et al. (2009). The N European Russia location in CLIMBER-2P time-to-equilibrium is around 35 kyr and full column soil carbon approaching 180 kg m^{-2} (Fig. 14). The Ayaha-Yacha modelled site in Wania et al. (2009b) has a time to equilibrium of greater than 80 kyr and soil carbon concentration of around 200 kg m^{-2}, the Zimov model predicts that 200 kg m^{-2} soil carbon concentrations can be reached within 10 kyr (even in the very cold region) for wet–dry conditions and 150 kg m^{-2} in 10 kyr for the dry–wet conditions. The total soil column

GMDD
7, 4931–4992, 2014

carbon concentration and time-to-equilibrium in this model is within the range of the Wania and Zimov models. Other dynamic settings are also within this range, with the possible exception of the xfast setting. The N. Canada (Fig. 14) location takes a longer time to reach equilibrium for the medium dynamic setting, more than 40 kyr, and has a full column soil carbon concentration of around 130 kg m^{-2}. This value is too high and does not agree with data, because this area of northern Canada was underneath the Laurentide ice sheet at LGM. Since the demise of the Laurentide ice sheet around 13 kyr ago (Denton et al., 2010) there has not been enough time for these soils to equilibrate. As well as this, this region has very high water contents (and islands) which are not represented in CLIMBER-2P which may modify soil carbon concentrations.

4.3 Soil carbon stocks

The total land carbon stocks were tuned using data from Ciais et al. (2012). An assumption made in this study is that all "extra" soil carbon, relative to the standard model, in the Arctic region is located in permafrost soils and only by the mechanism of increased soil carbon residence time in frozen soils. Table 5 shows the Ciais et al. (2012) land carbon pools values that have been used to tune this model. The standard model total land carbon (tlc) are similar to the active land carbon stocks, with LGM tlc at 2199 Gt C and PI tlc at 1480 Gt C (shown in Table 7).

The soil types that are found in the continuous and discontinuous permafrost zone are the Cryosols (circumpolar atlas) or Gelisols (Soil taxonomy). Within this group are further subgroups; Turbels which are subject to cryoturbation and characterise the continuous permafrost zone, Orthels which are less affected by cryoturbation and are related to discontinuous permafrost and Histels which relate to peat growth (histosols) and have permafrost at less than 2 m depth. Histels are not directly represented in the simplified model, as they are dominated by peat growth (Sphagnum), a distinct PFT not represented in CLIMBER-2P.

The Tarnocai et al. (2009) soil organic carbon concentration (socc) estimates for the present-day for relevant soils are shown in Table 6. Summing "All soils" with Loess

GMDD
7, 4931–4992, 2014

soils and Deltaic deposits gives the 1672 Gt C estimated total socc for the permafrost region. The extra land carbon stocks created in our model in permafrost soils range between 1339 to 1945 Gt C (Table 8) compared to Tarnocai et al. at 1672 Gt C and 1600 ± 300 Gt C in the Ciais et al. (2012) estimate for inert land carbon for the present day. For the LGM climate, the model shows a range of 1987 to 2117 Gt C for extra soil carbon compared to the Ciais estimate of 2300 ± 300 Gt C for inert land carbon. The "medium" dynamic setting shows total land carbon stocks in the present-day outside the range estimated by Ciais et al. (2012). However, during tuning (see Appendix B) this overestimate could not be improved upon.

4.4 Soil carbon concentration in the top 100 cm

The carbon content of Orthels and Turbels decreases with depth, but high carbon contents are still found at depths of 3 m and more (Tarnocai et al., 2009). For Orthels (with alluvium) around 80 % of their carbon content was found in the top 200 cm and for Turbels 38 % of carbon content was found in the top 100 cm. To compare the CLIMBER-2P output with ground spatial data, it is assumed that 40 % of the modelled total soil-column carbon is located in the top 100 cm for all permafrost affected soils.

Soil carbon data from Hugelius et al. (2013) was used to compare against the CLIMBER-2P output. The Orthels and Turbels dominate the continuous and coldest permafrost areas, with Histels and other soils becoming more dominant towards the southern parts of the permafrost region. As no peatlands or wetlands are represented in our simplified model, only Orthel and Turbel soils were used as comparison points for soil organic carbon concentration (socc). Socc data from Hugelius et al. (2013), for grid cells with 50 % or more Orthel and Turbel soils, was upscaled to the CLIMBER-2P grid. These mean socc data values for the top 1 m of soil were plotted against CLIMBER-2P model output for matching grid cells, this is shown in Fig. 15. Also shown in Fig. 15 is the standard model output, which has no permafrost mechanism. Two grid cells show very much higher socc than data suggests, with around a three fold overestimate and are located in Siberia. All other grid cells are within a range of ±80 % heavily dependent

GMDD
7, 4931–4992, 2014

on the soil carbon dynamic setting. The standard model shows progressively worse performance as mean socc increases in the data. The permafrost model shows an increasing socc trend more similar to data. Comparing the spatial location of socc to data can be done using Fig. 16. The two grid cells with very high socc compared to data are central and eastern Siberia. These grid cells are both 100 % permafrost and have had a total of 101 kyr (80k for LGM(eq) plus 21k to PI(tr)) years to accumulate carbon. This is in contrast to the North American continent grid cells which were underneath the ice sheet until the deglaciation, so have had less time to accumulate carbon.

The assumption that all permafrost region soil-carbon acts as Turbels and Orthels has an impact on the physical location of the socc with respect to data. Turbels and Orthels are located in the northern parts of the permafrost zone with Histels and other soils becoming more dominant to the south. Compared to socc in ground data (Fig. 16), a northern bias in socc is seen in model output, as expected. Histels (peatland soils) and other soil types of the permafrost zone, with an estimated 390 Gt C (Table 6) are not represented in our model. If these were modelled they should increase socc in model output in the more southern part of the permafrost region, and parts of Canada. Large river deltas, which contain deltaic deposits of 241 Gt C (Tarnocai et al., 2009) are also not represented in our model. One example of this is the Lena river delta, located in western Siberia which, combined with dominance of Histels in this region (Hugelius et al., 2013), cause a high socc in data. The model does not represent well the boreal forest belt (Fig. 4) which is also located in the southern region of the permafrost zone. This results in carbon input to soils in this region being underestimated in our model.

Figure 17 shows the model outputs for the LGM climate. No soil carbon is present underneath ice sheets and the highest carbon concentrations are seen in present day south-eastern Russia and Mongolia, with quite high soil carbon concentrations in present day northern Europe and north-western Russia. Comparing this output to the permafrost extent model (Fig. 13), the socc is likely located too far north for the same reasons as the PI(tr) socc but also because permafrost extent is underestimated for the LGM(eq) climate. The northern China region, according to data, was continuous

GMDD
7, 4931–4992, 2014

permafrost at LGM as was the south west Russia region. These regions would have higher socc in model output if the modelled permafrost area was closer to data estimates. The same would be true of the Siberian shelf. This means that the extra soil carbon tuned to the Ciais et al. (2012) estimate (Table 5) is concentrated in a central band in Eurasia more so than the model would predict if permafrost extent was more like the data estimate for LGM.

5 Model applications and limitations

5.1 Applications

The simplified permafrost mechanism is intended to be used for the study of carbon-cycle dynamics on timescales of centuries/millennia and longer. It represents an improvement on the previous terrestrial carbon cycle model in CLIMBER-2 which did not include any effects of frozen soils. It is not intended for the study of carbon cycle dynamics on scales shorter than centuries due to the simplifications made and many processes not accounted for in the simplified model.

5.2 Simplifications and limitations

The permafrost model does not make any changes to soil carbon based on hydrology or ice contents. Precipitation only affects vegetation growth, not soil formation.

No account is taken of the effect of peatland soils in permafrost regions as the PFT for Sphagnum species, which accounts for most of peat soil vegetation cover, is not included in the model. The effect of frozen ground inhibiting root growth (to depth) is not accounted for, which may have an impact on the GPP and soil formation in very cold regions.

During glacial climates, no extra land is exposed as sea-level drops in the CLIMBER-2P model, all the carbon used to tune the carbon dynamics for LGM period is located on land that is presently above sea-level.

GMDD
7, 4931–4992, 2014

Wetlands and river deltas increase the spatial spread of the soil carbon in the real world, and these are not represented in CLIMBER-2P. Therefore, it is also not intended that the spatial location of the highest soil carbon concentrations should be used as a very good indicator of the real world case.

The model has no soil "depth" (only a carbon pool) so ^{14}C cannot be used as a useful tracer as part of CLIMBER-2P in its current configuration. The CLIMBER-2P model does have a ^{13}C tracer within the carbon cycle which is intended to be used in conjunction with the permafrost model to constrain carbon cycle dynamics.

The possible impact of high dust concentrations on soil formation during glacial climates is not accounted for in the model. Loess soils, those created by wind-blown dust or alluvial soils, are not represented. For our study it is assumed that the ratio of loess to non-loess soils is the same in the present day as it was during glacial climates. This is not the case in the real World, where high dust concentrations in the dry atmosphere increased Loess deposition at LGM (Frechen, 2011). However, the LGM climate is only representative of the coldest and driest period of the last glacial. Evidence suggests that soils were productive in cold conditions in the permafrost region of the last glacial period with loess accumulation only more widely significant towards the harsh conditions of the LGM (Elias and Crocker, 2008; Chlachula and Little, 2009; Antoine et al., 2013; Willerslev et al., 2014).

No changes were made to the vegetation model or to controls on soil input which are only dependent upon temperature and NPP, the Mammoth-Steppe biome is not explicitly modelled (Zimov et al., 2012).

Underneath ice-sheets soil carbon is zero, as an ice sheet extends over a location with soil carbon (and vegetation), that carbon is released directly into the atmosphere. As an ice sheet retreats and exposes ground, the vegetation (and soil) can start to grow again. So, our model does not account for any carbon that may have been buried underneath ice sheets (Wadham et al., 2012).

GMDD
7, 4931–4992, 2014

6 Conclusions/summary

This permafrost-carbon model is a simplified representation of the general effect of frozen ground on soil carbon decay. In the presence of frozen ground the soil carbon decays more slowly. The method by which permafrost is diagnosed relies only on the balance between warm (above 0 °C) and cold (below 0 °C) days, which removes the problem of compounding errors in thermal diffusion calculations (for example). As such, the permafrost-carbon model would perform just as well in distant past climates as it does in pre-industrial climate. In order to account for uncertainties in carbon accumulation and release rates in frozen (and thawing) soils, a range of dynamic settings are retained which agree with total land carbon estimates of Ciais et al. (2012). Due to the slow accumulation in permafrost soils, soil carbon has a long time to equilibrium and therefore the present-day climate must be treated as a transient state, not as an equilibrium state. We showed the model performs reasonably well at pre-industrial present-day conditions. The permafrost-carbon model creates a mechanism which slowly accumulates soil carbon in cooling or cold climates and quickly releases this high soil carbon in warming climates, caused either by changes in insolation patterns or by global increases in temperature and climatic changes due to greenhouse gas feedbacks and ocean circulation changes. It can thus be used to quantitatively evaluate the role of permafrost dynamics on the carbon build-up and release associated with this specific physical environment, over supra-centennial to glacial–interglacial timescales.

Appendix A: Snow correction

A1 Linear model

In more complex physical models, snow correction of ground temperature is achieved by modelling the thermal diffusion characteristics of the snow cover; a function of snow depth and snow type (for example snow density). A thermal diffusion model is used

GMDD
7, 4931–4992, 2014

to make an estimate of the snow–ground interface temperature using the surface air temperature, the thermal gradient is also dependent upon the initial snow–ground interface temperature. Within the CLIMBER-2 model, snow is already modelled (Petoukhov et al., 2000) as it has a significant effect on overall climate (Vavrus, 2007). Snow depth in CLIMBER-2 is available as well as snow fraction per cell, but snow type and snow density is not individually modelled. Attempting to model the thermal diffusion in the snow does not make sense for CLIMBER-2, as with permafrost location. Rather the approach is to use measurement data to create a general relationship between air temperature and snow–ground interface temperature based only on the snow depth.

The snow correction linear model is based on data from Taras et al. (2002) giving a correction for snow–ground interface temperature from snow depth and air temperature. Figure A1a shows the data from Taras et al. (2002) and the linear regressions (labelled as A, B and C) of this data re-plotted per snow depth (Fig. A1b). Equation (A1) shows this linear model for snow correction, which is only applied for surface air temperatures lower than −6 °C. This snow–ground interface temperature is used to calculate the freeze index (DDF_{sc}) in Eq. (4) in the main text.

$$T_{\text{g.i.}} = T_{\text{surf}} - \frac{(T_{\text{surf}} + 6) \cdot \text{SD}}{100} \tag{A1}$$

Where $T_{\text{g.i.}}$ is ground interface temperature (°C), T_{surf} is surface air temperature (°C) and SD is snow depth (cm).

A2 Snow correction validation

This simple snow-correction was tested against data from Morse and Burn (2010). Figure A2 shows the error made by the linear model when used to predict the snow–ground interface temperature (or snow depth temperature) from Morse and Burn measurement data. In the more extreme conditions, the error of the linear model is far higher, for example in deep snow and cold temperatures. Figure A3 shows the outputs from CLIMBER-2 for snow depths plotted against surface air temperatures for the

GMDD
7, 4931–4992, 2014

PI(eq) pre-industrial climate (green circles) and LGM(eq) glacial climate (blue squares) for all grid cells. The large CLIMBER-2 grid size means that extreme conditions are not present in the model output. Comparing Figs. A2 and A3 shows that the linear correction can provide an estimated confidence within −8 °C for the deepest snow cover and highest temperatures of CLIMBER-2P data output, and within +-2 °C for the majority of CLIMBER-2P data outputs. A similar performance is found when comparing to snow thickness and snow–ground interface temperatures from Zhang (2005) for a site in Zyryanka, Russia. The most extreme temperatures and snow conditions produce a larger error from the linear model, but the intermediate conditions, those seen in CLIMBER-2P data points, agree better with the data. Overall the effect of the snow correction within the model produced a maximum decrease in permafrost area of 8 % (compared to the uncorrected version) in the most affected grid cell for the PI(eq) simulation and is therefore significant.

Appendix B: Tuning for total land carbon at the LGM and PI

Table B1 shows all the settings for "*a*" and "*b*" per soil pool (Eq. 3, main text) that were tested to obtain total soil carbon contents for the LGM and the PI simulations. Figure B1 shows the modelled total land carbon (Gt C) for all simulations sorted by permafrost area function. Green dashed lines on the LOW–MEDIUM area setting indicate the dynamic settings chosen to represent the "slow", "medium", "fast" and "extra-fast" permafrost-carbon dynamic settings. The total land carbon content is clearly very sensitive to permafrost area, and despite many simulation tunings only the LOW–MEDIUM area setting provided a good enough range of dynamics that could be used to later investigate the permafrost-carbon dynamics. Within the settings chosen, the "medium" dynamic setting overestimated the present-day total land carbon estimate from Ciais et al. (2012), but further tuning experiments did not improve this over-estimate.

Acknowledgements. The research leading to these results has received funding from the European Community's Seventh Framework Programme (FP7 2007–2013) under Grant 238366

GMDD
7, 4931–4992, 2014

(GREENCYCLES II) and under grant GA282700 (PAGE21, 2011–2015). D. M. Roche is supported by INSU-CNRS and by NWO under project no. 864.09.013.

References

Aleksandrova, L. N.: Processes of humus formation in soil, in: Proceedings of Leningrad Agricultural Institute, Leningrad, 142, 26–82, 1970 (in Russian).

Alexeev, V. A., Nicolsky, D. J., Romanovsky, V. E., and Lawrence, D. M.: An evaluation of deep soil configurations in the CLM3 for improved representation of permafrost, Geophys. Res. Lett., 34, L09502, doi:10.1029/2007GL029536, 2007.

Antoine, P., Rousseau, D. D., Degeai, J. P., Moine, O., Lagroix, F., Fuchs, M., and Lisá, L.: High-resolution record of the environmental response to climatic variations during the Last Interglacial–Glacial cycle in Central Europe: the loess-palaeosol sequence of Dolní Věstonice (Czech Republic), Quaternary Sci. Rev., 67, 17–38, 2013.

Bouttes, N., Roche, D. M., and Paillard, D.: Impact of strong deep ocean stratification on the glacial carbon cycle, Paleooceanography, 24, PA3202, doi:10.1029/2008PA001707, 2009.

Bouttes, N., Paillard, D., Roche, D. M., Brovkin, V., and Bopp, L.: Last Glacial Maximum CO_2 and $\delta^{13}C$ succesfully reconciled, Geophys. Res. Lett., 38, L02705, doi:10.1029/2010GL044499, 2011.

Bouttes, N., Paillard, D., Roche, D. M., Waelbroeck, C., Kageyama, M., Lourantou, A., Michel, E., and Bopp, L.: Impact of oceanic processes on the carbon cycle during the last termination, Clim. Past, 8, 149–170, doi:10.5194/cp-8-149-2012, 2012.

Brovkin, V., Ganopolski, A., and Svirezhev, Y.: A continuous climate–vegetation classification for use in climate–biosphere studies, Ecol. Model., 101, 251–261, 1997.

Brovkin, V., Ganopolski, A., Archer, D., and Rahmstorf, S.: Lowering of glacial atmospheric CO_2 in repsonse to changes in oceanic circulation and marine biogeochemistry, Paleoceanography, 22, PA4202, doi:10.1029/2006PA001380, 2007.

Chlachula, J. and Little, E.: A high-resolution Late Quaternary climatostratigraphic record from Iskitim, Priobie Loess Plateau, SW Siberia, Quaternary Int., 240, 139–149, 2011.

Ciais, P., Tagliabue, A., Cuntz, M., Bopp, L., Scholze, M., Hoffman, G., Lourantou, A., Harrison, S. P., Prentice, I. C., Kelley, D. I., Koven, C., and Piao, S. L.: Large inert carbon

GMDD
7, 4931–4992, 2014

pool in the terrestrial biosphere during the Last Glacial Maximum, Nat. Geosci., 5, 74–79, doi:10.1038/NGEO1324, 2012.
Collins, M., Knutti, R., Arblaster, J., Dufresne, J.-L., Fichefet, T., Friedlingstein, P., Gao, X., Gutowski, W. J., Johns, T., Krinner, G., Shongwe, M., Tebaldi, C., Weaver, A. J., and Wehner, M.: Long-term climate change: projections, commitments and irreversibility, in: Climate Change 2013: The Physical Science Basis. Contribution of Working Group I to the Fifth Assessment Report of the Intergovernmental Panel on Climate Change, edited by: Stocker, T. F., Qin, D., Plattner, G.-K., Tignor, M., Allen, S. K., Boschung, J., Nauels, A., Xia, Y., Bex, V., and Midgley, P. M., Cambridge University Press, Cambridge, UK and New York, NY, USA, 2013.
Dankers, R., Burke, E. J., and Price, J.: Simulation of permafrost and seasonal thaw depth in the JULES land surface scheme, The Cryosphere, 5, 773–790, doi:10.5194/tc-5-773-2011, 2011.
Denton, G. H., Anderson, R. F., Toggweiler, J. R., Edwards, R. L., Schaefer, J. M., and Putnam, A. E.: The last glacial termination, Science, 328, 1652–1656, 2010.
Ekici, A., Beer, C., Hagemann, S., Boike, J., Langer, M., and Hauck, C.: Simulating high-latitude permafrost regions by the JSBACH terrestrial ecosystem model, Geosci. Model Dev., 7, 631–647, doi:10.5194/gmd-7-631-2014, 2014.
Elias, S. A. and Crocker, B.: The Bering Land Bridge: a moisture barrier to the dispersal of steppe–tundra biota?, Quaternary Sci. Rev., 27, 2473–2483, 2008.
Fischer, H., Schmitt, J., Lüthi, D., Stocker, T. F., Tschumi, T., Parekh, P., Kohler, P., Völker, C., Gersonde, R., Barbante, C., Le Floch, M., Raynaud, D., and Wolff, E.: The role of Southern Ocean processes in orbital and millennial CO_2 variations – a synthesis, Quaternary Sci. Rev., 29, 193–205, 2010.
Frechen, M.: Loess in Eurasia, Quaternary Int., 234, 1–3, 2011.
French, H. M. and Millar, S. W. S.: Permafrost at the time of the Last Glacial Maximum (LGM) in North America, Boreas, 43, 667–677, doi:10.1111/bor.12036, 2013.
Ganopolski, A., Petoukhov, V., Rahmstorf, S., Brovkin, V., Claussen, M., Eliseev, A., and Kubatzki, C.: CLIMBER-2: a climate system model of intermediate complexity. Part II: model sensitivity, Clim. Dynam., 17, 735–751, 2001.
Gouttevin, I., Menegoz, M., Dominé, F., Krinner, G., Koven, C., Ciais, P., Tarnocai, C., and Boike, J.: How the insulating properties of snow affect soil carbon distribution in the continen-

GMDD
7, 4931–4992, 2014

tal pan-Arctic area, J. Geophys. Res.-Biogeo., 117, G02020, doi:10.1029/2011JG001916, 2012.
Harden, J. W., Koven, C. D., Ping, C. L., Hugelius, G., McGuire, A. D., Cammill, P., Jorgenson, T., Kuhry, P., Michaelson, G. J., O'Donnell, J. A., Schuur, E. A. G., Tarnocai, C., Johnson, K., and Grosse, G.: Field information links permafrost carbon to physical vulnerabilities of thawing, Geophys. Res. Lett., 39, L15704, doi:10.1029/2012GL051958, 2012.
Hugelius, G., Tarnocai, C., Broll, G., Canadell, J. G., Kuhry, P., and Swanson, D. K.: The Northern Circumpolar Soil Carbon Database: spatially distributed datasets of soil coverage and soil carbon storage in the northern permafrost regions, Earth Syst. Sci. Data, 5, 3–13, doi:10.5194/essd-5-3-2013, 2013.
Jones, A., Stolbovoy, V., Tarnocai, C., Broll, G., Spaargaren, O., and Montanarella, L. (Eds.): Soil Atlas of the Northern Circumpolar Region, European Commission, Office for Official Publications of the European Communities, Luxembourg, 142 pp., 2009.
Koven, C., Friedlingstein, P., Ciais, P., Khvorostyanov, D., Krinner, G., and Tarnocai, C.: On the formation of high-latitude soil carbon stocks: effects of cryoturbation and insulation by organic matter in a land surface model, Geophys. Res. Lett., 36, L21501, doi:10.1029/2009GL040150, 2009.
Koven, C., Riley, W. J., and Stern, A.: Analysis of permafrost thermal dynamics and response to climate change in the CMIP5 Earth System Models, J. Climate, 26, 1877–1900, 2013.
Levavasseur, G., Vrac, M., Roche, D. M., Paillard, D., Martin, A., and Vandenberghe, J.: Present and LGM permafrost from climate simulations: contribution of statistical downscaling, Clim. Past, 7, 1225–1246, doi:10.5194/cp-7-1225-2011, 2011.
Lourantou, A., Lavric, J. V., Kohler, P., Barnola, J. M., Paillard, D., Michel, E., Raynaud, D., and Chappelaz, J.: Constraint of the CO_2 rise by new atmospheric carbon isotopic measurements during the last deglaciation, Global Biogeochem. Cy., 24, BG2015, doi:10.1029/2009GB003545, 2010.
Maslin, M. A. and Thomas, E.: Balancing the deglacial global carbon budget: the hydrate factor, Quaternary Sci. Rev., 22, 1729–1736, 2003.
Monnin, E., Indermühle, A., Dällenbach, A., Flückiger, J., Stauffer, B., Stocker, T. F., Raynaud, D., and Barnola, J. M.: Atmospheric CO_2 concentrations over the last glacial termination, Science, 291, 112–114, 2001.
Morse, P. D. and Burn, C. R.: Ground Temperature Variation with Snow, Kendall Island Bird Sanctuary, Outer Mackenzie Delta, Northwest Territories, GEO2010, 2010.

GMDD
7, 4931–4992, 2014

Nelson, F. E. and Outcalt, S. I.: A computational method for perdiction and regionalization of permafrost, Arctic Alpine Res., 19, 279–288, 1987.
Peltier, W. R.: Global glacial isostasy and the surface of the ice-age Earth: the ICE-5G (VM2) Model and GRACE, Annu. Rev. Earth Pl. Sc., 32, 111–149, doi:10.1146/annurev.earth.32.082503.144359, 2004.
Petoukhov, V., Ganopolski, A., Brovkin, V., Claussen, M., Eliseev, A., Kubatzki, C., and Rahmstorf, S.: CLIMBER-2: a climate system model of intermediate complexity. Part 1: model description and performance for present climate, Clim. Dynam., 16, 1–17, 2000.
Prentice, I. C., Harrison, S. P., and Bartlein, P. J.: Global vegetation and terrestrial carbon cycle changes after the last ice age, New Phytol., 189, 988–998, 2011.
Riseborough, D., Shiklomanov, N., Etzelmuller, B., Gruber, S., and Marchenko, S.: Recent advances in permafrost modelling, Permafrost Periglac., 19, 137–156, 2008.
Rodionov, A., Flessa, H., Grabe, M., Kazansky, O. A., Shibistova, O., and Guggenberger, G.: Organic carbon and total nitrogen variability in permafrost-affected soils in a forest tundra ecotone, Eur. J. Soil Sci., 58, 1260–1272, 2007.
Saito, K., Sueyoshi, T., Marchenko, S., Romanovsky, V., Otto-Bliesner, B., Walsh, J., Bigelow, N., Hendricks, A., and Yoshikawa, K.: LGM permafrost distribution: how well can the latest PMIP multi-model ensembles perform reconstruction?, Clim. Past, 9, 1697–1714, doi:10.5194/cp-9-1697-2013, 2013.
Schmitt, J., Schneider, R., Elsig, J., Leuenberger, D., Lourantou, A., Chappellaz, J., Kohler, P., Joos, F., Stocker, T. F., Leuenberger, M., and Fischer, H.: Carbon isotope constraints on the deglacial CO_2 rise from ice cores, Science, 336, 711–714, 2012.
Schuur, E. A.: High risk of permafrost thaw, Nature, 480, 32–33, 2011.
Schuur, E. A. G., Bockheim, J., Canadell, J. G., Euskirchen, E., Field, C. B., Goryachkin, S. V., Hagemann, S., Kuhry, P., Lafleur, P. M., Lee, H., Mazhitova, G., Nelson, F. E., Rinke, A., Romanovsky, V. E., Shiklomanov, N., Tarnocai, C., Venevsky, S., Vogel, J. G., and Zimov, S.: Vulnerability of permafrost carbon to climate change: implications for the global carbon cycle, Bioscience, 58, 8, 701–714, 2008.
Schuur, E. A. G., Vogel, J. G., Crummer, K. G., Lee, H., Sickman, J. O., and Osterkamp, T. E.: The effect of permafrost thaw on old carbon release and net carbon exchange from tundra, Nature, 459, 556–559, doi:10.1038/nature08031, 2009.

GMDD
7, 4931–4992, 2014

Shakun, J. D., Clark, P. U., He, F., Marcott, S. A., Mix, A. C., Liu, Z., Otto-Bliesner, B., Schmittner, A., and Bard, E.: Global warming preceded by increasing carbon dioxide concentrations during the last deglaciation, Nature, 484, 49–54, 2012.

Sigman, D. M., Hain, M. P., and Haug, G. H.: The polar ocean and glacial cycles in atmospheric CO_2 concentration, Nature, 466, 47–55, 2010.

Stocker, T. F., Qin, D., Plattner, G.-K., Tignor, M., Allen, S. K., Boschung, J., Nauels, A., Xia, Y., Bex, V., and Midgley, P. M.: IPCC, 2013: Climate Change 2013: The Physical Science Basis. Contribution of Working Group I to the Fifth Assessment Report of the Intergovernmental Panel on Climate Change Cambridge University Press, Cambridge, UK and New York, NY, USA, 1535 pp., 2013.

Taras, B., Sturm, M., and Liston, G. E.: Snow–ground interface temperatures in the Kupuruk River Basin, Arctic Alaska: measurements and model, J. Hydrometeorol., 3, 377–394, 2002.

Tarnocai, C., Canadell, J. G., Schuur, E. A. G., Kuhry, P., Mazhitova, G., and Zimov, S.: Soil organic carbon pools in the northern circumpolar permafrost region, Global Biogeochem. Cy., 23, GB2023, doi:10.1029/2008GB003327, 2009.

van Huissteden, J. and Dolman, A. J.: Soil carbon in the Arctic and the permafrost carbon feedback, Environmental Sustainability, 4, 545–551, 2012.

Vandenberghe, J., Renssen, H., Roche, D. M., Goosse, H., Velichko, A. A., Gorbunov, A., and Levavasseur, G.: Eurasia permafrost instability constrained by reduced sea-ice cover, Quaternary Sci. Rev., 34, 16–23, doi:10.1016/j.quascirev.2011.12.001, 2012.

Vavrus, S.: The role of terrestrial snow cover in the climate system, Clim. Dynam., 29, 73–88, doi:10.1007/s00382-007-0226-0, 2007.

Wadham, J. L., Arndt, S., Tulaczyk, S., Stibal, M., Tranter, M., Telling, J., Lis, G. P., Lawson, E., Ridgwell, A., Dubnick, A., Sharp, M.J., Anesio, A. M., and Butler, C. E. H.: Potential methane reservoirs beneath Antarctica, Nature, 488, 633–637, 2012.

Wania, R., Ross, I., and Prentice, I. C.: Intergrated peatlands and permafrost into a dynamic global vegetation model: 1. Evaluation and sensitivity of physical land surface processes, Global Biogeochem. Cy., 23, GB3014, doi:10.1029/2008GB003412, 2009a.

Wania, R., Ross, I., and Prentice, I. C.: Intergrated peatlands and permafrost into a dynamic global vegetation model: 2. Evaluation and sensitivity of vegetation and carbon cycle processes, 23, GB3015, doi:10.1029/2008GB003413, 2009b.

Willerslev, E., Davison, J., Moora, M., Zobel, M., Coissac, E., Edwards, M. E., Lorenzen, E. D., Vestergård, M., Gussarova, G., Haile, J., Craine, J., Gielly, L., Boessenkool, S., Epp, L. S.,

GMDD
7, 4931–4992, 2014

Pearman, P. B., Cheddadi, R., Murray, D., Bråthen, K. A., Yoccoz, N., Binney, H., Cruaud, C., Wincker, P., Goslar, T., Alsos, I. G., Bellemain, E., Brysting, A. K., Elven, R., Sønstebø, J. H., Murton, J., Sher, A., Rasmussen, M., Rønn, R., Mourier, T., Cooper, A., Austin, J., Möller, P., Froese, D., Zazula, G., Pompanon, F., Rioux, D., Niderkorn, V., Tikhonov, A., Savvinov, G., Roberts, R. G., Macphee, R. D. E., Gilbert, M. T. P., Kjær, K. H., Orlando, L., Brochmann, C., and Taberlet, P.: Fifty thousand years of Arctic vegetation and megafaunal diet, Nature, 506, 47–51, 2014.

Yu, Z., Loisel, J., Brosseau, D. P., Beilman, D. W., and Hunt, S. J.: Global peatland dynamics since the Last Glacial Maximum, Geophys. Res. Lett., 37, L13402, doi:10.1029/2010GL043584, 2010.

Zech, R., Huang, Y., Zech, M., Tarozo, R., and Zech, W.: High carbon sequestration in Siberian permafrost loess-paleosols during glacials, Clim. Past, 7, 501–509, doi:10.5194/cp-7-501-2011, 2011.

Zhang, T.: Global Annual Freezing and Thawing Indices, National Snow and Ice Data Center, Boulder, Colorado, USA, 1998.

Zhang, T.: Influence of the seasonal snow cover on the ground thermal regime. An overview, Rev. Geophys., 43, RG4002, doi:10.1029/2004RG000157, 2005.

Zhang, T., Heginbottom, J. A., Barry, R. G., and Brown, J.: Further statistics on the distribution of permafrost and ground ice in the Northern Hemisphere, Polar Geography, 24, 126–131, doi:10.1080/10889370009377692, 2000.

Zhao, M., Running, S., Heinsch, F. A., and Nemani, R.: MODIS-derived terrestrial primary production, in: Land Remote Sensing and Global Environmental Change, Springer, New York, 635–660, 2011.

Zimov, N. S., Zimov, S. A., Zimova, A. E., Zimova, G. M., Chuprynin, V. I., and Chapin III, F. S.: Carbon storage in permafrost and soils of the mammoth tundra–steppe biome: role in the global carbon budget, Geophys. Res. Lett., 36, L02502, doi:10.1029/2008GL036332, 2009.

Zimov, S. A., Zimov, N. S., Tikhonov, A. N., and Chapin III, F. S.: Mammoth steppe: a high-productivity phenomenon, Quaternary Sci. Rev., 57, 26–45, 2012.

GMDD
7, 4931–4992, 2014

Table 1. Simulated climates used in this study to develop, tune and validate the permafrost-carbon mechanism.

Date	Event
LGM (equilibrium)	Obtained after an 80 kyr spin-up with glacial CO_2 levels of 190 ppmv, reduced ocean volume, LGM ice sheets, LGM insolation, LGM runoff. Carbonate compensation in the ocean (Brovkin et al., 2002). Sea-level effects on coast lines are not included, land area is as PI (equilibrium). The continental shelves exposed at LGM are not accounted for in this model set-up because the fate of any carbon that may have accumulated on these shelves is not well constrained. The long time of spin-up, 80 kyr, is required to allow the soil carbon pools to equilibrate.
PI (equilibrium)	Obtained after 40 kyr spin-up with pre-industrial CO_2 levels of 280 ppmv, present-day ocean volume, present-day ice sheets, insolation, and land run-off. The 40 kyr spin-up time allows soil carbon pools to equilibrate.
PI (transient)	End of a 21 kyr simulation of a transient deglaciation that has the LGM equilibrium climate as a start point at 21 kyr BP. The PI (transient) is the climate at 0 yr BP. The transient deglaciation has evolving ice sheets scaled to sea-level, increasing ocean volume, insolation changes (seasonality), carbonate compensation and LGM runoff. This transient PI climate is required to account for the long time to equilibrium of the permafrost affected soil carbon pools. In order to compare model output with ground-data the PI(transient) provides a more realistic model output.

GMDD
7, 4931–4992, 2014

Table 2. Permafrost area model settings for Eq. (6).

	A	β
HIGH	0.58	$22(F_{sc} - 0.58)$
MED	0.555	$21(F_{sc} - 0.59)$
LOW–MED	0.54	$20.5(F_{sc} - 0.595)$
LOW	0.53	$20(F_{sc} - 0.6)$

GMDD
7, 4931–4992, 2014

Table 3. Selected settings for permafrost decay function, where subscript indicates the soil pool. Permafrost area model is LOW–MEDIUM for all.

Dynamic settings	Constants settings for Eq. (3)			
	a_{fast}	b_{fast}	a_{slow}	b_{slow}
Slow	10	10	10	10
Medium	20	40	1	3
Fast	60	50	0	1
Xfast	60	80	0.1	0.1

GMDD
7, 4931–4992, 2014

Table 4. Modelled permafrost-affected land area and data based estimates.

	Permafrost area ($\times 10^6$ km^2) (land underlain by permafrost)		
Permafrost model area setting	Pre-Industrial climate (equilibrium)	Pre-Industrial climate (transient)	Glacial climate
LOW–MEDIUM	14.0	18.4	20.7
Data estimate	12.21 to 16.98 (Zhang et al., 2000)		33.8 (Levavasseur et al., 2011) 40 (Vandenberghe et al., 2012)

GMDD
7, 4931–4992, 2014

Table 5. Total land carbon stock estimates from Ciais et al. (2012).

Period	Total land carbon (Gt C)	Active land carbon (Gt C)	Inert land carbon (Gt C)
Present-day	3970 ± 325	2370 ± 125	1600 ± 300
LGM	3640 ± 400	1340 ± 500	2300 ± 300

GMDD
7, 4931–4992, 2014

Table 6. Permafrost region soil carbon stock estimates from Tarnocai et al. (2009).

Soil type	depth		Soil carbon (Gt C)
Gelisols	To 1 m	Turbels	211.9
		Orthels	51.3
		Histels	88.0
		All	351.5
	To 3 m	Turbels	581.3
		Orthels	53.0
		Histels	183.7
		All	818.0
All soils	To 1 m		495.8
	To 3 m		1024.0
Pleistocene loess	> 3 m		407
Deltaic	> 3 m		241

GMDD
7, 4931–4992, 2014

Table 7. Modelled total land carbon stocks per model setting.

Total land carbon (Gt C)	Standard model	With permafrost, per dynamic setting			
		slow	medium	fast	xfast
PI(transient)	2199	4052	4425	4079	3819
LGM(eq)	1480	3597	3563	3467	3481

GMDD
7, 4931–4992, 2014

Table 8. Modelled permafrost-region extra land carbon stocks wrt. standard model per model setting.

Extra soil carbon (Gt C)	Standard model	With permafrost, per dynamic setting			
		slow	medium	fast	xfast
PI (transient)	0	1853	2226	1880	1620
LGM (eq)	0	2117	2083	1987	2001

GMDD
7, 4931–4992, 2014

Table A1. All settings for Eq. (3) (main article) used to tune total land carbon and permafrost-carbon dynamics.

Area: LOW

	a_{fast}	b_{fast}	a_{slow}	b_{slow}
1	30	30	2	2
2	40	30	2	2
3	50	50	2	2
4	50	50	3	3
5	20	20	10	10
6	10	10	20	20
7	55	45	3	2
8	70	60	0	1
9	60	70	2	2
10	80	70	0	1
11	100	90	0	1
12	150	100	0	0.5
13	100	150	0	0.5
14	75	200	0	0.5
15	20	20	2	2
16	60	50	0	1

Area: LOW–MED

	a_{fast}	b_{fast}	a_{slow}	b_{slow}
1	50	40	0	0.5
2	21	20	2	2
3	10	10	10	10
4	60	50	0	1
5	50	60	0	1
6	10	30	1	3
7	20	40	1	3
8	5	50	1	3
9	30	70	0	1
10	50	5	3	1
11	45	30	3	2
12	45	25	3	2
13	40	20	3	2
14	60	80	0.1	0.1
15	10	40	1	4
16	5	55	1	2

Area: MED

	a_{fast}	b_{fast}	a_{slow}	b_{slow}
1	50	40	0	0.5
2	20	20	2	2
3	10	10	10	10
4	30	50	0	0.5
5	60	50	0	1

Area: HIGH

	a_{fast}	b_{fast}	a_{slow}	b_{slow}
1	30	30	2	2
2	15	30	1	2
3	15	15	15	15
4	10	30	0	1
5	5	45	0	2
6	4	8	12	16
7	8	35	0	1
8	3	8	12	16
9	1	35	1	2
10	30	10	1	1
11	0.5	40	0.5	2.5
12	3	7	11	15
13	0.2	45	0.2	3
14	1	100	0	1
15	20	30	0	1
16	70	40	0	0.5
17	20	20	2	2
18	60	50	0	1

GMDD
7, 4931–4992, 2014

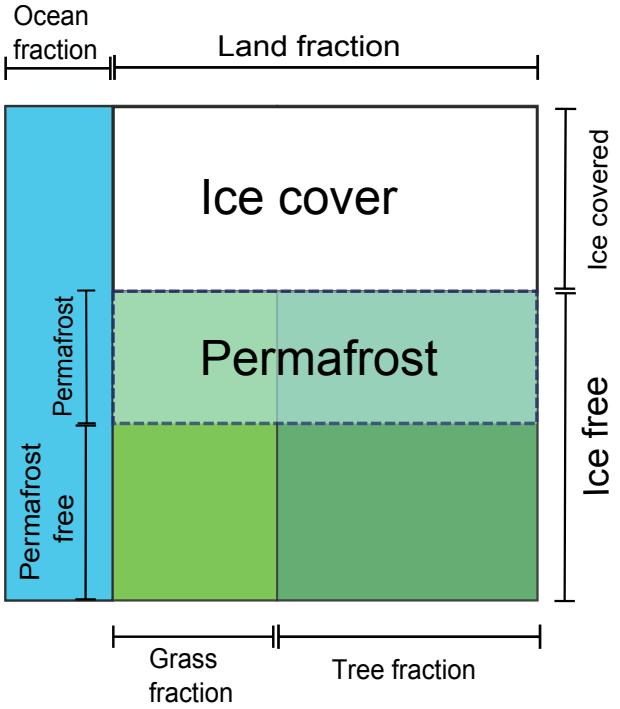

Figure 1. A CLIMBER-2P grid cell showing the distribution of different cell cover types.

GMDD
7, 4931–4992, 2014

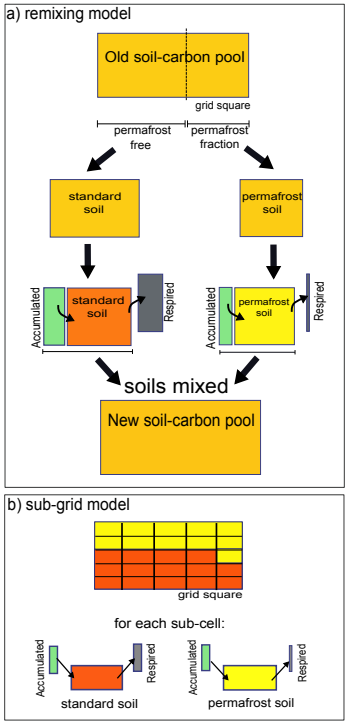

Figure 2. Schematic of a CLIMBER-2P grid cell showing how carbon is accumulated at each time-step. Re-mixing model **(a)** separates grid cell into permafrost or non permafrost, calculates the change in carbon pool and re-mixing all carbon in the cell back together. Sub-grid model **(b)** separates the grid cell into 25 sub-grid cells and calculates change in carbon pool in each individually and does not re-mix any carbon between sub-grid cells.

GMDD
7, 4931–4992, 2014

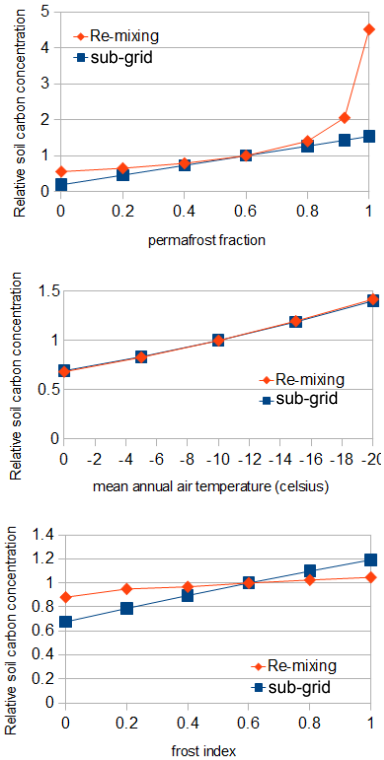

Figure 3. 1-D model output to compare the performance of the re-mixing (diamonds) and the sub-grid (squares) approaches. Top: MAAT (mean annual air temperature) and frost-index are constant, permafrost-fraction is variable. Middle: frost-index and permafrost-fraction are constant, MAAT is variable. Bottom: permafrost-fraction and MAAT are constant, frost index is variable. Input to soils from plant mortality and rainfall are constant for all.

GMDD
7, 4931–4992, 2014

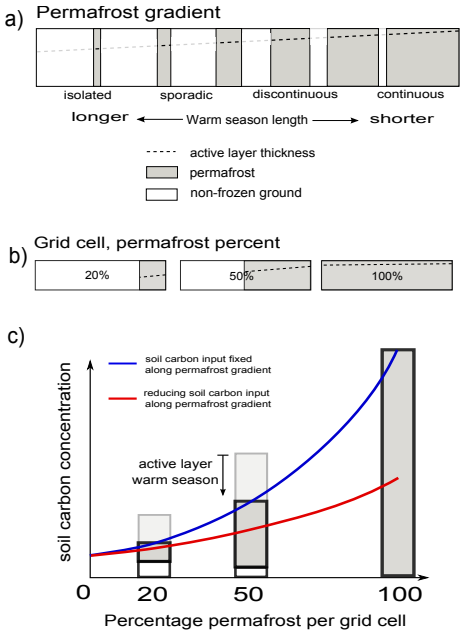

Figure 4. (a) Schematic representation of a permafrost gradient, active layer thickens as permafrost coverage reduces, warm season lengthens as permafrost reduces **(b)** example modelled grid cells for permafrost percentage and active layer thickness, **(c)** schematic relationship between permafrost coverage per grid cell and equilibrium soil carbon concentration. Here MAT and Frost index are considered fixed for all cases. Increased active layer and increased warm season length in turn increase soil carbon decay and therefore reduce equilibrium soil carbon concentration. Reducing NPP along the permafrost gradient, so reducing carbon input to soils, would oppose this effect.

GMDD
7, 4931–4992, 2014

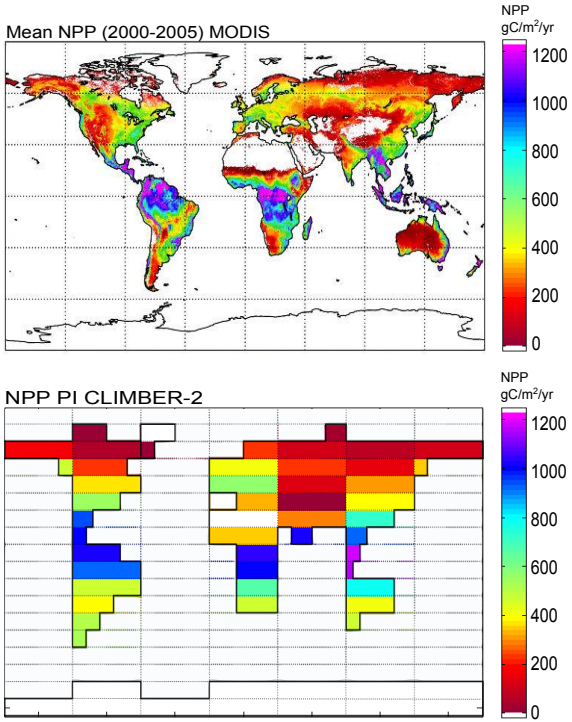

Figure 5. Comparison of NPP (net primary productivity), which has a control on carbon input to soils, for MODIS dataset (top) and CLIMBER-2 model for PI(eq) plotted on the same scale ($g\,C\,m^{-2}\,yr^{-1}$).

GMDD
7, 4931–4992, 2014

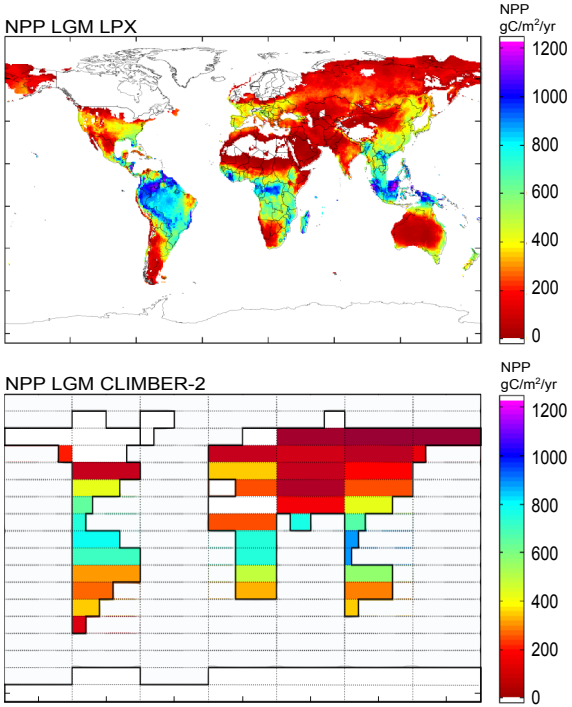

Figure 6. Comparison of NPP (net primary productivity), which has a control on carbon input to soils, for LPX model (top, courtesy M Martin-Calvo) and CLIMBER-2 model for LGM(eq) plotted on the same scale ($g\,C\,m^{-2}\,yr^{-1}$), and same scale as Fig. 4.

GMDD
7, 4931–4992, 2014

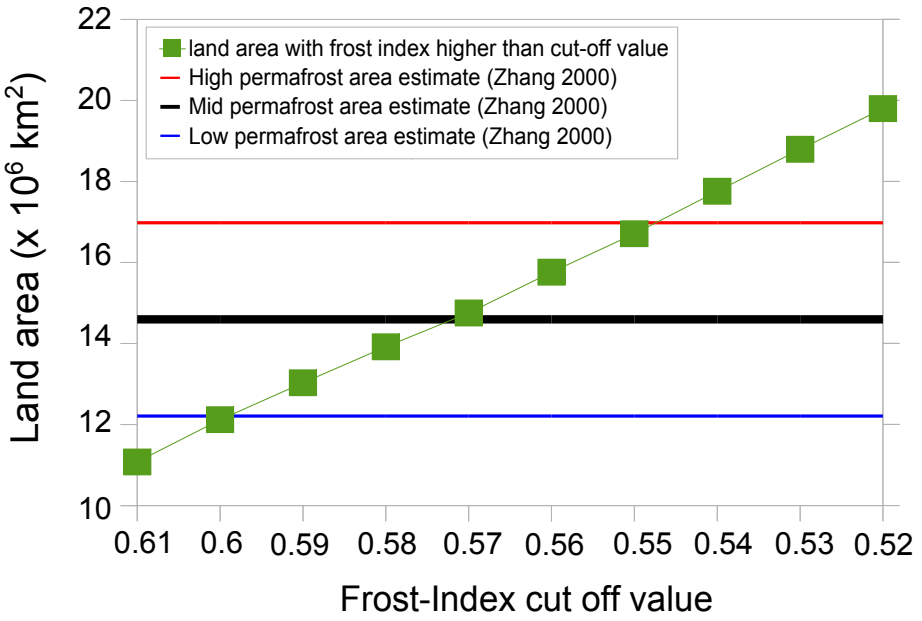

Figure 7. Total land area with a frost-index higher (colder) than the *x* axis cut-off value, for frost-index data from Zhang (1998) (NSIDC). Shown in horizontal lines are the Zhang et al. (2000) data estimates for area of land underlain by permafrost.

GMDD
7, 4931–4992, 2014

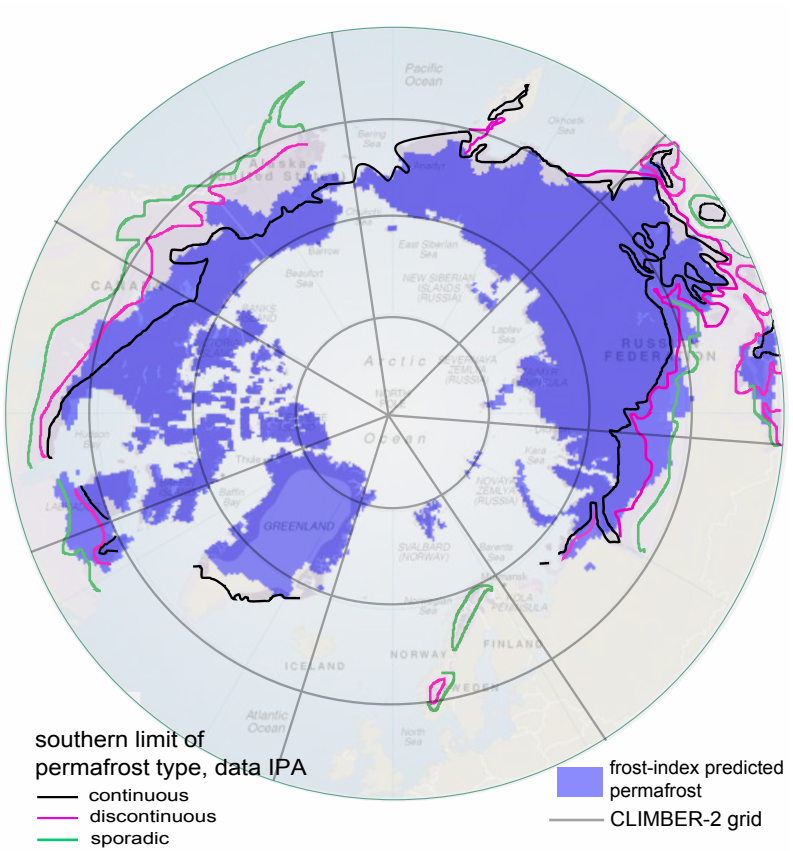

Figure 8. Map of land with frost-index greater than 0.57 (frost-index predicted permafrost) shown in blue with southern limit of permafrost boundaries for the present day defined by IPA overlaid. Black line: continuous permafrost, pink line: discontinuous permafrost, green line: sporadic permafrost. Grey lines are the CLIMBER-2 grid.

GMDD
7, 4931–4992, 2014

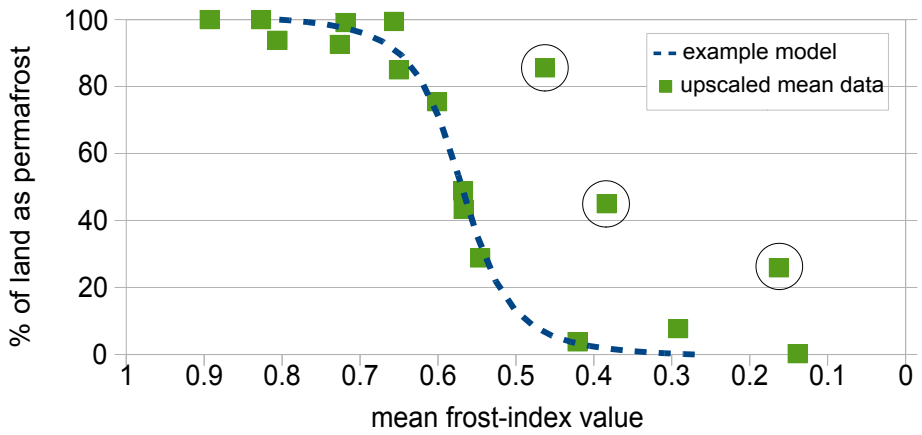

Figure 9. Frost-index predicted permafrost fraction of land from Fig. 8 upscaled to the CLIMBER-2 grid and plotted against mean Frost-index for the same CLIMBER-2 grid cell. Circled points are where the total fraction of land vs. ocean in the grid cell are small (land is less that 25 % of the grid cell) and ocean temperatures pull frost-index lower (warmer). Blue dashed line is a representative relationship between frost-index and permafrost land-fraction.

GMDD
7, 4931–4992, 2014

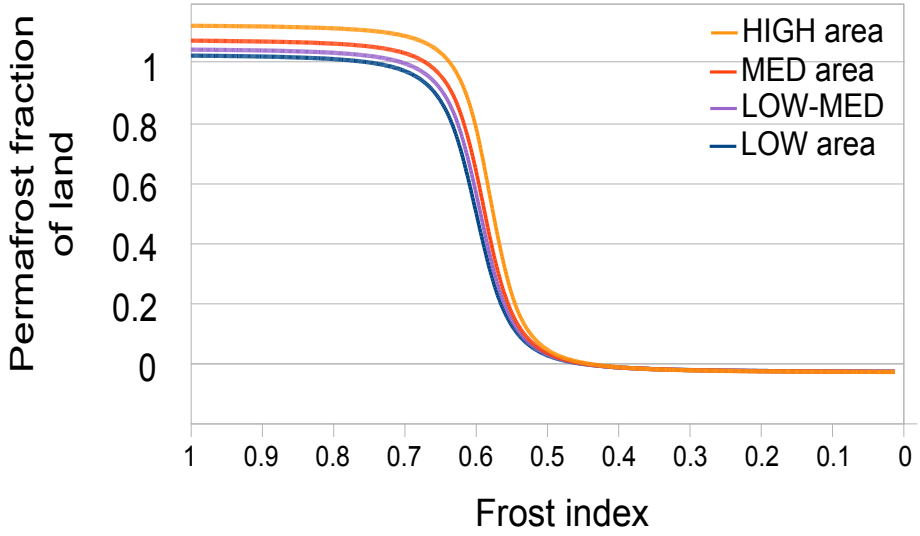

Figure 10. CLIMBER-2P model for permafrost-fraction of the land in a grid cell from frost-index (snow corrected). Range of areas are within the range of estimates for present-day land area underlain by permafrost by Zhang et al. (2000). Fraction is limited between 0 and 1.

GMDD
7, 4931–4992, 2014

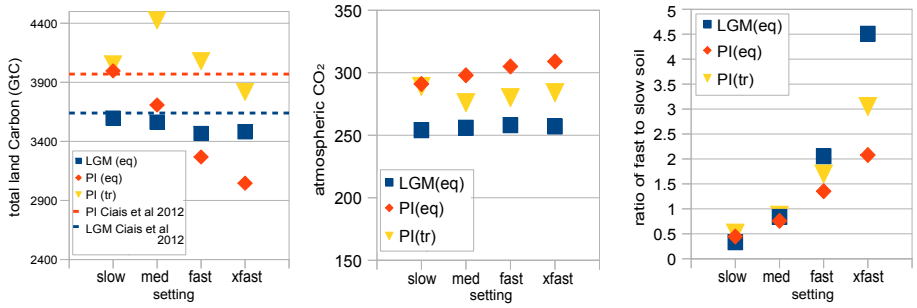

Figure 11. Chosen dynamic settings for the range of permafrost-carbon dynamics. Left: total land carbon with Ciais et al. (2012) estimates as dashed lines. Middle: atmospheric CO_2 (ppm). Right: ratio of all fast to all slow soil pools indicating the speed of response of the soil carbon to changing climate.

GMDD
7, 4931–4992, 2014

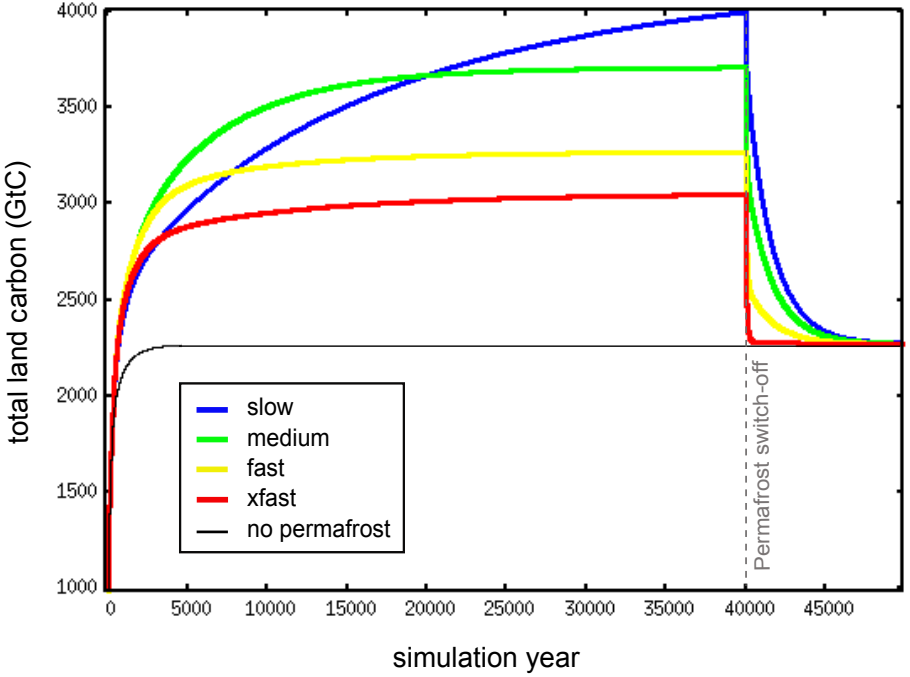

Figure 12. Total land carbon (Gt C) for the PI(eq) simulation followed by a permafrost switch-off at 40k sim years representing a complete and immediate permafrost thaw demonstrating the different dynamic behaviour of each dynamic setting.

GMDD
7, 4931–4992, 2014

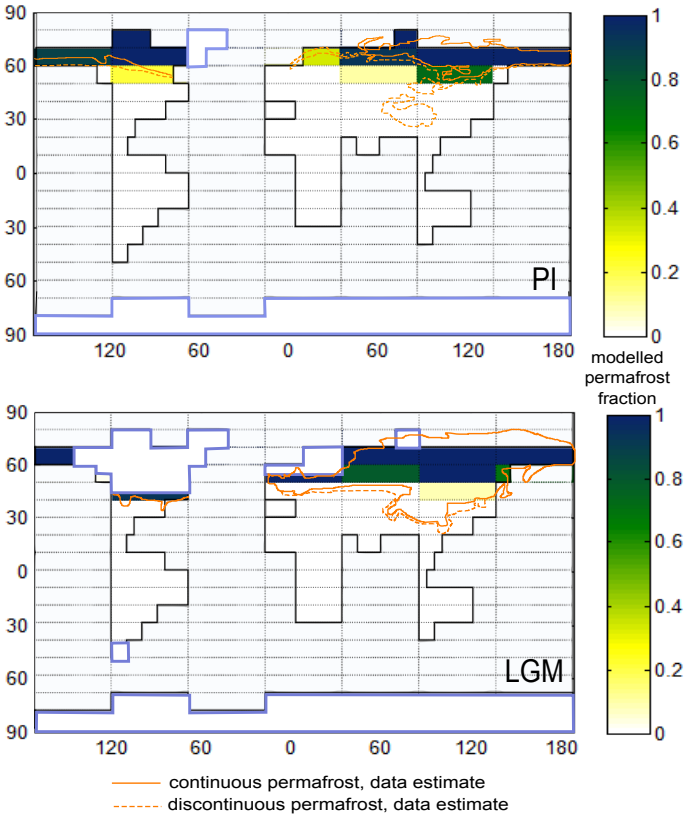

Figure 13. Modelled permafrost area for top: PI(tr) simulation, bottom LGM(eq) simulation for LOW–MEDIUM permafrost area. Overlaid in orange are data estimates from Circumpolar Atlas (Jones et al., 2009) for present-day, Vandenberghe et al. (2008) for LGM Eurasia, French and Millar (2013) for LGM N. America.

GMDD
7, 4931–4992, 2014

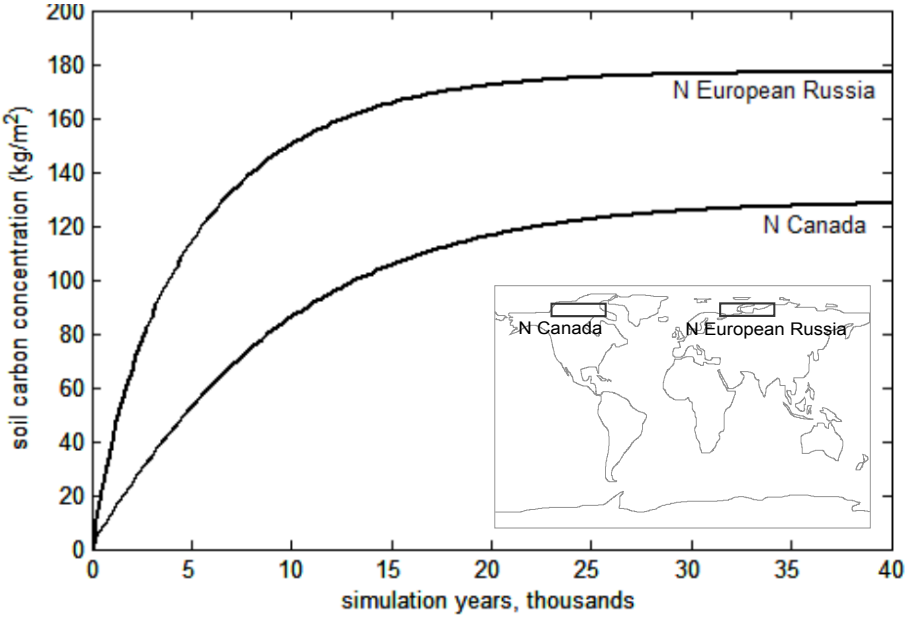

Figure 14. modelled PI(eq) simulation output for total soil column carbon concentration for two grid cells. Permafrost-carbon dynamic setting is medium.

GMDD
7, 4931–4992, 2014

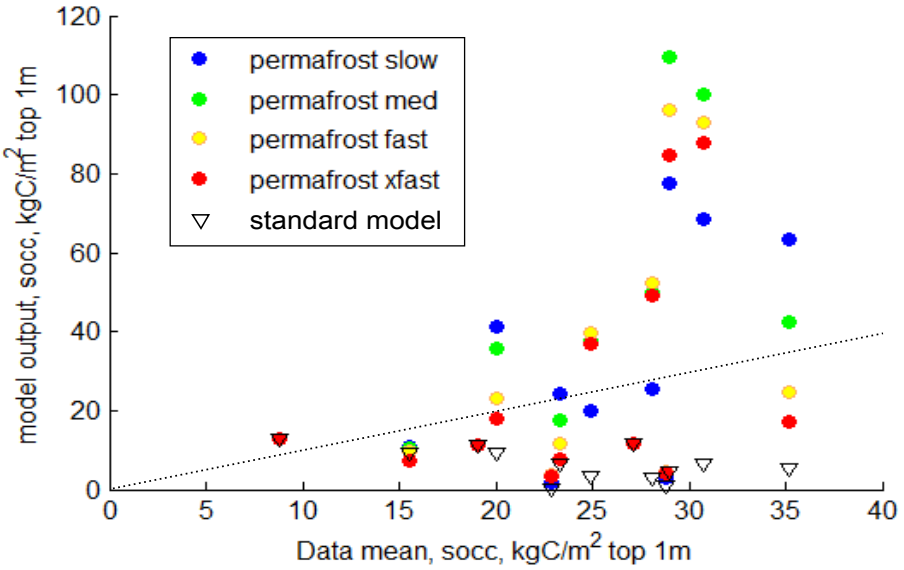

Figure 15. Modelled socc for the top 1 m plotted against socc data for the top 1 m of soil upscaled to the CLIMBER-2 grid scale. Circles are for permafrost-carbon model (CLIMBER-2P), triangles are for the standard model (CLIMBER-2). Dashed line shows the 1 : 1 position. Points are socc kg C m^{-2}

GMDD
7, 4931–4992, 2014

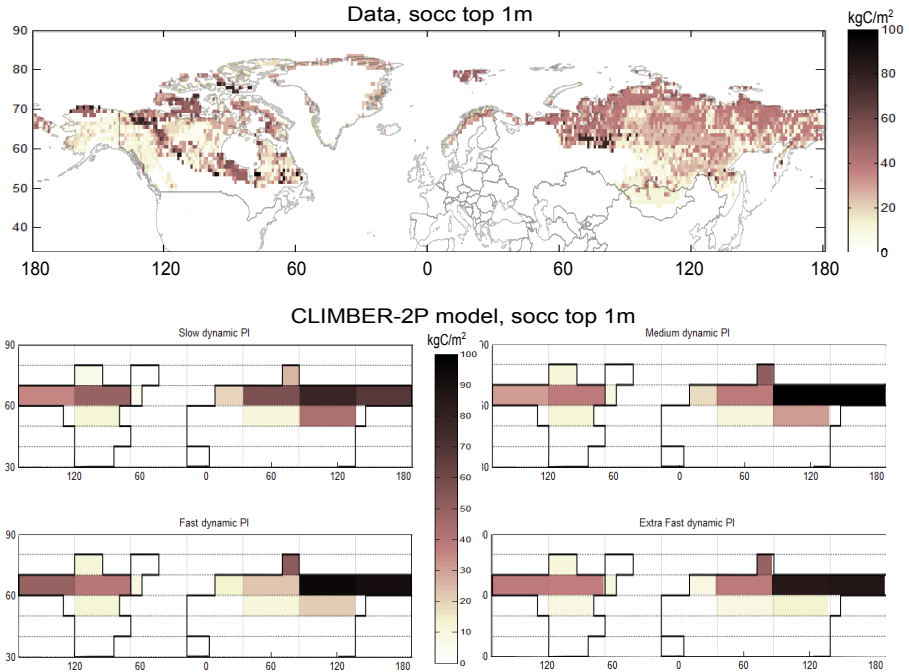

Figure 16. Socc data (kg C m^{-2}) for the top 100 cm of soils, Hugelius et al. (2013) (top). Modelled PI(tr) socc (kg C m^{-2}) in permafrost soils for top 100 cm (lower four).

GMDD
7, 4931–4992, 2014

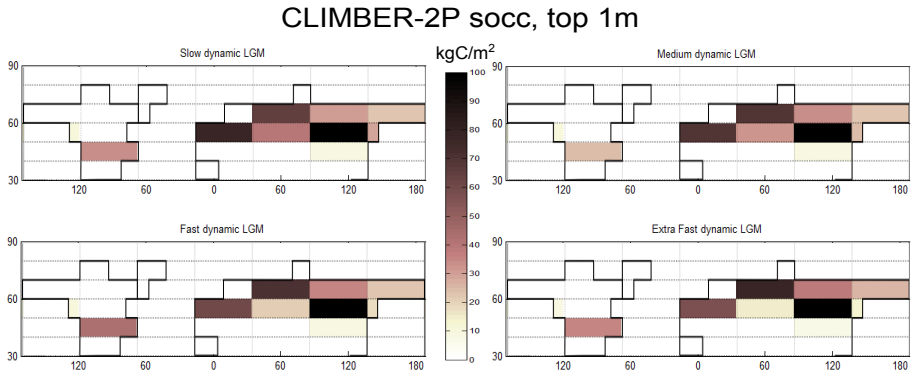

Figure 17. Modelled LGM(eq) socc (kg C m^{-2}) in permafrost soils for top 100 cm.

GMDD
7, 4931–4992, 2014

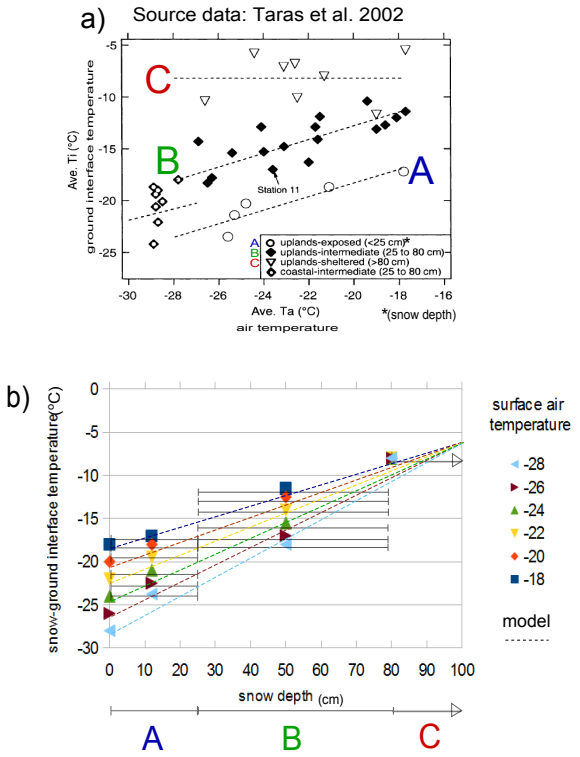

Figure A1. Snow correction model **(b)**. Linear regressions of data points in **(a)** (dashed lines) are re-plotted as ground interface temperature per snow depth and shown in **(b)**. For each surface air temperature, a linear model based on snow depth predicts the snow–ground interface temperature.

GMDD
7, 4931–4992, 2014

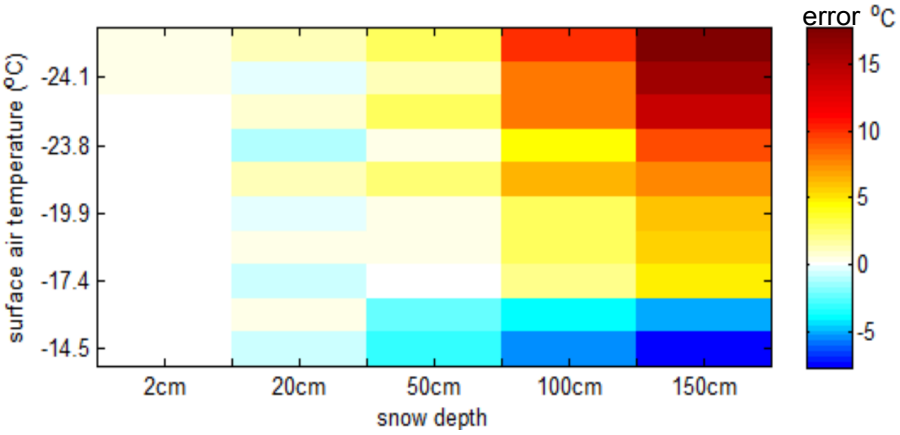

Figure A2. Model error when the linear snow correction model is used to predict temperatures at snow-depth or snow–ground interface for data from Morse and Burn (2010). Positive numbers indicate the linear model output is too warm compared to data.

GMDD
7, 4931–4992, 2014

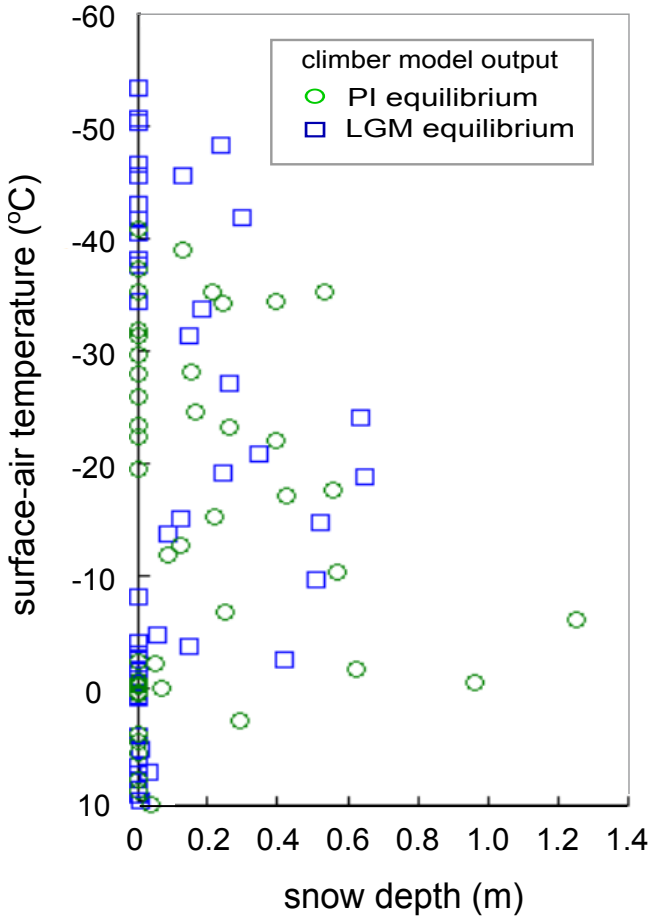

Figure A3. CLIMBER-2 model output for snow depth (m) plotted against surface air temperature (˚C) for the PI(eq) (green circles) and LGM(eq) (blue squares) climates. Model output does not show extreme conditions for snow cover due to the very large grid-cell size.

GMDD
7, 4931–4992, 2014

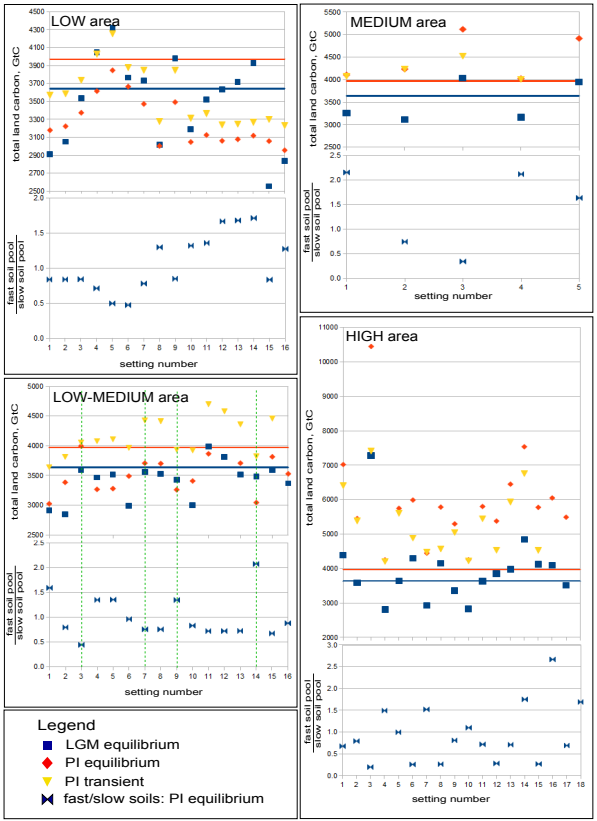

Figure B1. Modelled total land carbon stocks, and ratio of fast soils to slow soils for all settings used to tune the permafrost-carbon dynamics. Blue squares are for the LGM(eq) simulation, red diamonds are for the PI(eq) simulation and yellow triangles are for the PI(tr) simulation. Horizontal lines show the total land carbon estimates of Ciais et al. (2012). Green dashed lines indicate the chosen dynamic settings where LGM(eq) and PI(tr) show best agreement with Ciais et al. (2012) estimates.

GMDD
7, 4931–4992, 2014